

AD-A040 843

UNITED TECHNOLOGIES RESEARCH CENTER EAST HARTFORD CONN F/G 20/4
A STUDY OF THE TURBULENT SHOCK WAVE BOUNDARY LAYER INTERACTION.(U)
FEB 77 R LEVY, S J SHAMROTH, H J GIBELING F33615-73-C-4119

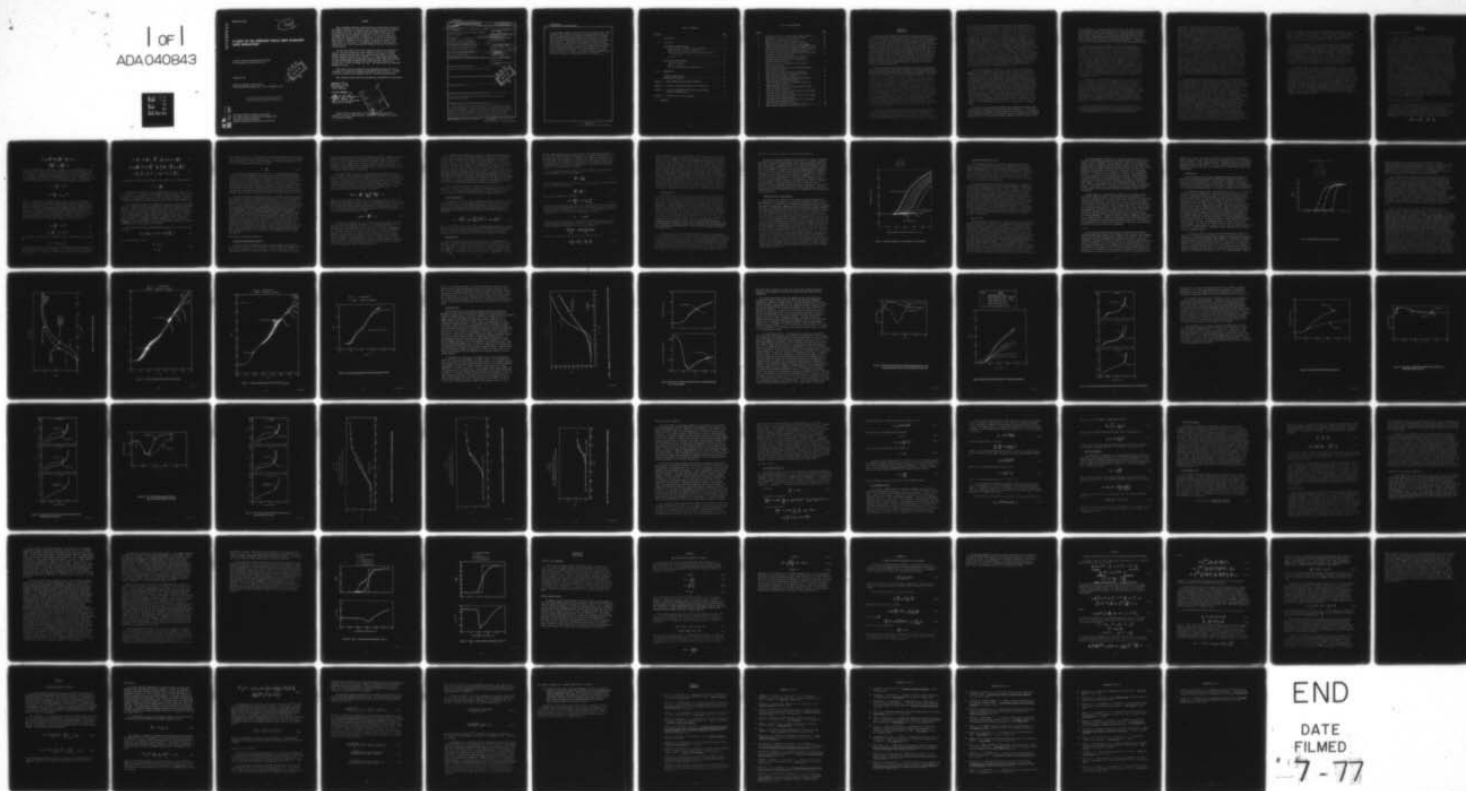
UNCLASSIFIED

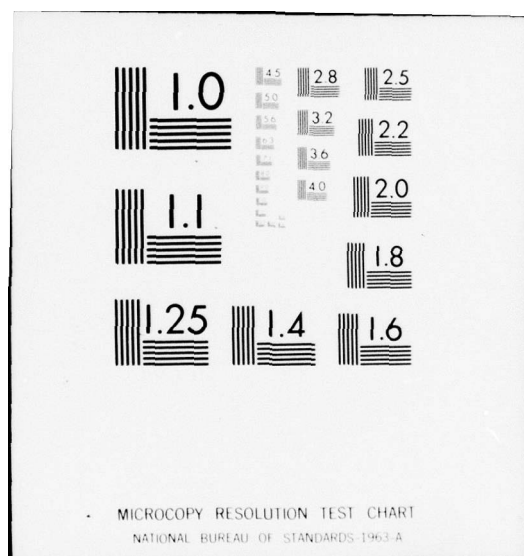
UTRC/R76-911729-15

AFFDL-TR-76-163

NL

1 of 1
ADA040843





ADA 040843

AFFDL-TR-76-163

12
NW

A STUDY OF THE TURBULENT SHOCK WAVE BOUNDARY LAYER INTERACTION

UNITED TECHNOLOGIES RESEARCH CENTER
EAST HARTFORD, CONNECTICUT 06108

FEBRUARY 1977

TECHNICAL REPORT AFFDL-TR-76-163
FINAL REPORT FOR PERIOD JULY 1, 1973 - OCTOBER 25, 1976

DDC
JUN 21 1977
RECEIVED

Approved for public release; distribution unlimited

AD No. _____
DDC FILE COPY

AIR FORCE FLIGHT DYNAMICS LABORATORY
AIR FORCE WRIGHT AERONAUTICAL LABORATORIES
AIR FORCE SYSTEMS COMMAND
WRIGHT-PATTERSON AIR FORCE BASE, OHIO 45433

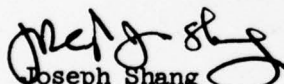
NOTICE

When Government drawings, specifications, or other data are used for any purpose other than in connection with a definitely related Government procurement operation, the United States Government thereby incurs no responsibility nor any obligation whatsoever; and the fact that the government may have formulated, furnished, or in any way supplied the said drawings, specifications, or other data, is not to be regarded by implication or otherwise as in any manner licensing the holder or any other person or corporation, or conveying any rights or permission to manufacture, use, or sell any patented invention that may in any way be related thereto.

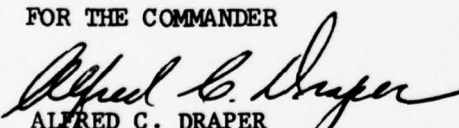
The work described in this Final Technical Report was supported by the U.S. Air Force through Dr. Wilbur Hankey of the Air Force Systems Command, Wright-Patterson AFB, Ohio, under Contract F33615-73-C-4119, Project 70640307, and Work Unit 23070419. Dr. Joseph Shang (AFFDL/FXM) was the contract monitor and the work covered by this report was performed at United Technologies Research Center, East Hartford, Connecticut, between July 1, 1973 and October 25, 1976. The final report was submitted February 18, 1977.

This report has been reviewed by the Information Office (10) and is releasable to the National Technical Information Service (NTIS). At NTIS, it will be available to the general public, including foreign nations.

This technical report has been reviewed and is approved for publication.


Joseph Shang
Project Engineer

FOR THE COMMANDER


ALFRED C. DRAPER
Asst for Research & Technology
Aeromechanics Division

ACCESSION for	File	Box	✓
NTIS	Doc	Box	✓
UNANNOUNCED			
JUSTIFICATION			
BY	DISTRIBUTION/AVAILABILITY CODES		
Dist.	Avail. Code	Spec.	
A			

Copies of this report should not be returned unless return is required by security considerations, contractual obligations, or notice on a specific document.

UNCLASSIFIED

SECURITY CLASSIFICATION OF THIS PAGE (When Data Entered)

REPORT DOCUMENTATION PAGE		READ INSTRUCTIONS BEFORE COMPLETING FORM	
1. REPORT NUMBER AFFDL-7R-76-163	2. GOVT ACCESSION NO.	3. RECIPIENT'S CATALOG NUMBER 1 Jul 73-25 Oct 76	
4. TITLE (and Subtitle) A Study of the Turbulent Shock Wave Boundary Layer Interaction.	5. TYPE OF REPORT & PERIOD COVERED Final Report, July 1, 1973-October 25, 1976		
7. AUTHOR(s) Ralph/Levy, Stephen J./Shamroth, Howard J./Gibeling, Henry/McDonald	6. PERFORMING ORG. REPORT NUMBER R76-911729-15		
9. PERFORMING ORGANIZATION NAME AND ADDRESS United Technologies Research Center East Hartford, Connecticut 06118	8. CONTRACT OR GRANT NUMBER(s) F33615-73-C-4119		
11. CONTROLLING OFFICE NAME AND ADDRESS Air Force Flight Dynamics Laboratory Air Force Systems Command Wright-Patterson Air Force Base, Ohio 45433	10. PROGRAM ELEMENT, PROJECT, TASK AREA & WORK UNIT NUMBERS Project 70640307 Work Unit 23070419		
14. MONITORING AGENCY NAME & ADDRESS (if different from Controlling Office)	12. REPORT DATE February 18, 1977		
	13. NUMBER OF PAGES 74		
	15. SECURITY CLASS. (of this report) Unclassified		
16. DISTRIBUTION STATEMENT (of this Report) Approved for Public Release; Distribution Unlimited.			
17. DISTRIBUTION STATEMENT (of the abstract entered in Block 20, if different from Report)			
18. SUPPLEMENTARY NOTES			
19. KEY WORDS (Continue on reverse side if necessary and identify by block number) Viscous-Inviscid Interaction, Shock Wave-Boundary Layer Interaction, Navier-Stokes Solutions.			
20. ABSTRACT (Continue on reverse side if necessary and identify by block number) Two approaches to the shock wave-boundary layer interaction procedure have been investigated. In the first approach a strong interaction boundary layer procedure has been applied to the shock wave-turbulent boundary layer interaction problem by modifying a well-proven weak interaction boundary layer procedure to allow for strong interaction solutions. The modifications included the incorporation of an outer flow interaction model and the revision			

DD FORM 1 JAN 73 1473

EDITION OF 1 NOV 65 IS OBSOLETE

UNCLASSIFIED


SECURITY CLASSIFICATION OF THIS PAGE (When Data Entered)

409252

UNCLASSIFIED

SECURITY CLASSIFICATION OF THIS PAGE(When Data Entered)

20.

of the governing equations to allow for flow in separated regions. When a turbulence model originally developed for attached boundary layers was used, poor agreement was found between calculations and data. However, when a modified turbulence model, based upon computational turbulence studies and recent experimental data was used, considerably better agreement was obtained. The original weak interaction solution procedure, the modifications made under the current effort, and sample calculations are presented in this report. In the second approach the feasibility of using a fully implicit Navier-Stokes solution procedure for the interaction problem was investigated. The results indicate that the fully implicit procedure is a promising one, however, further development work, particularly in regard to shock representation, is required. 

UNCLASSIFIED

ii

SECURITY CLASSIFICATION OF THIS PAGE(When Data Entered)

TABLE OF CONTENTS

<u>Section</u>	<u>Page</u>
I. INTRODUCTION.	1
II. DISCUSSION.	6
THE BOUNDARY LAYER APPROACH	6
Weak Interaction Boundary Layer Procedure.	6
Modifications For Strong Interaction	9
Solution Of The Strong Interaction Boundary Layer	
Equations	14
Results.	17
THE NAVIER-STOKES APPROACH.	41
The Basic Analysis	42
Method of Solution	47
Results of Navier-Stokes Computations.	48
III. CONCLUSIONS	54
BOUNDARY LAYER ANALYSIS	54
NAVIER-STOKES ANALYSIS.	54
APPENDIX A: WEAK INTERACTION CALCULATION PROCEDURE	55
APPENDIX B: BOUNDARY LAYER MODIFICATIONS FOR δ^* SPECIFIED.	57
APPENDIX C: ORIGINAL TURBULENCE MODEL USING THE TURBULENCE	
KINETIC ENERGY EQUATION	59
APPENDIX D: THE MINT CALCULATION PROCEDURE	63
IV. REFERENCES	69

LIST OF ILLUSTRATIONS

<u>Figure</u>		<u>Page</u>
1	Departure Solutions to the Boundary Layer Equations	15
2	Experimental Free Interaction Pressure Rise	19
3	Laminar Free Interaction Calculations	21
4	Laminar Calculation Branch Control Using Kick	22
5	Laminar Calculation Branch Control Using X _{CORNER}	23
6	Laminar Strong Interaction Flow Over Compression Corner . .	24
7	Separating Turbulent Strong Interaction Solution Using Weak Interaction Turbulence Modeling Assumptions	26
8	Comparison of Equilibrium and TKE Options For Attached Boundary Layer Turbulence Model	27
9	Wake Mixing Length Distribution with Attached Boundary Layer Turbulence Model Including Low Reynolds Number Correction	29
10	Sensitivity of Free Interaction to Turbulence Modeling Assumptions	30
11	Mixing Length Distributions with Attached Boundary Layer Turbulence Model	31
12	Free Interaction Wall Pressure Distributions	33
13	"Equilibrium" Wake Mixing Length Distributions with Low Reynolds Number Correction	34
14	"Equilibrium" Normal Mixing Length Distributions with Low Reynolds Number Corrections	35
15	"TKE" Wake Mixing Length Distributions with Low Reynolds Number Correction	36
16	"TKE" Normal Mixing Length Distributions with Low Reynolds Number Corrections	37
17	Turbulent Strong Interaction Solution For 19.67° Ramp Using Modified Turbulence Model	38
18	Turbulent Strong Interaction Solution For 16.06° Ramp Using Modified Turbulence Model	39
19	Turbulent Strong Interaction Solution For 9.81° Ramp Using Modified Turbulence Model	40
20	Navier-Stokes Interaction Calculation, $P_2/P_1 = 2$	52
21	Navier-Stokes Interaction Calculation, $P_2/P_1 = 3$	53

SECTION I

INTRODUCTION

Viscous-inviscid interaction flow fields are common occurrences found both on high Mach number flight vehicles and in supersonic or transonic turbomachinery. In general, the interaction may result either from the impingement of a shock wave upon a boundary layer or from a boundary layer developing along a compression surface. The resulting flow field is a complex phenomenon governed by the mutual interaction of a viscous inner shear layer and a nominally inviscid outer flow. Since viscous-inviscid interactions may lead to high drag losses, loss of control effectiveness, and very high local heating rates, and since such interactions commonly occur on high Mach number flight vehicles, a method to predict the interaction flow field accurately would be a valuable asset to the vehicle design team. The interaction flow field occurring in most cases of practical interest involves a turbulent boundary layer and, thus, a calculation procedure capable of accurately modeling turbulent boundary layer development should form the basis of the interaction prediction procedure.

Following Prandtl, the now classical method of solving viscous boundary layer-type problems first calculates a streamwise pressure distribution from purely inviscid considerations and then calculates the boundary layer development under the influence of this inviscid pressure distribution. No attempt is made to correct the inviscid pressure calculation for viscous effects originating in the boundary layer region. Obviously, such a two-step procedure can be valid only if the pressure distribution calculated ignoring viscous effects is a sufficiently good approximation to the pressure distribution which actually occurs. In many cases of practical interest, the inviscid pressure distribution is an excellent approximation to physical reality and in these cases the classical two-step procedure is valid. However, in certain flow situations which are termed strong interaction flows, the viscous displacement effects near the body surface are sufficiently large to cause the pressure distribution calculated ignoring viscous wall effects to be in serious error and in these cases the classical two-step boundary layer calculation procedure is invalid. The shock wave boundary layer interaction represents a common type of strong interaction flow. For such a flow, a prediction procedure which can be used with confidence must account for the mutual interaction between the inner viscous flow and the outer nominally inviscid flow.

Most interaction flow field procedures which have been developed and are discussed in the open literature have extended classical boundary layer theory to account for the mutual interaction phenomena. Under this approach the boundary layer equations which represent the inner flow field are solved simultaneously with an equation representing the outer flow field

thus including the required mutual interaction in the solution process. Most strong interaction solutions of the boundary layer equations are based conceptually upon the original work of Crocco and Lees (Ref. 13) as modified by Lees and Reeves (Ref. 27). In brief, Lees and Reeves solved a set of integral laminar boundary layer equations under the constraint that the flow angle at the outer edge of the boundary layer as determined by the boundary layer equations be equal to the flow angle at the outer edge of the boundary layer as determined by the inviscid flow field equations. This constraint was expressed through an equation relating the outer edge flow angle as determined by the continuity equation to the angle determined by the Prandtl-Meyer law. The use of an additional equation allowed the streamwise static pressure distribution to be calculated simultaneously with the boundary layer development and, thus, the streamwise static pressure distribution emerged as part of the solution as it should. The Lees and Reeves procedure resulted in fairly good predictions of static pressure through the interaction region for laminar boundary layer development on adiabatic walls; however, the prediction of skin friction, although qualitatively correct, showed significant quantitative disagreement with experimental data. The Lees and Reeves integral theory was extended to nonadiabatic walls by Klineberg and Lees (Ref. 24) and Holden (Ref. 22).

Although the analyses of Refs. 27, 22 and 24 have proven capable of predicting the streamwise pressure distribution through the interaction region, they are all based upon integral solutions of the equations and, thus, are limited in their generality. A more general solution for the interaction problem has been developed by Reyhner and Flugge-Lotz (Ref. 41) who replaced the integral boundary layer equations with the boundary layer partial differential equations of motion thus eliminating the constraints imposed by the profile assumptions required by integral solutions. Since the boundary layer equations calculated by spatial marching procedures are unstable in regions of reversed flow, the finite difference algorithm was modified so that in the separated flow region the streamwise convective terms were ignored or given a false positive convection velocity to maintain numerical stability. Being a full finite-difference solution rather than an integral solution, the Reyhner and Flugge-Lotz procedure is more general than integral calculation procedures; however, like integral procedures, the Reyhner-Flugge-Lotz procedure is still confined to laminar flow.

A solution of the turbulent boundary layer equations for strong interactions has been presented by Bertke, Werle and Polak (Ref. 5) who solved a set of equations originally developed by Werle and Vatsa (Ref. 55) for laminar flows. The method of Ref. 55 is a pseudo-time relaxation scheme that allows a direct specification of the downstream boundary conditions without having to adjust

initial parameters. A turbulence model that had been developed for attached weak interaction boundary layer flows was used. When this method was applied to the turbulent free interaction problem, the calculated plateau pressures were found to be approximately 30 percent higher than available data correlations. Bertke, Werle, and Polak attributed the discrepancy in predicted plateau pressure to limitations of the turbulence model used. A broad review of shock wave-boundary layer interaction solutions has been compiled by Hankey (Ref. 21).

Although until recently numerical viscous-inviscid interaction calculations were based almost entirely upon extended boundary layer procedures, the rapid development of both numerical techniques and computer capability now have made it practical to apply Navier-Stokes calculation procedures to the interaction problem. Since the Navier-Stokes equations represent the exact equations of motion, they contain no approximations other than those made in connection with turbulence modeling. For example, the assumption of constant pressure at any streamwise station which is inherent in most boundary layer procedures and which may be in serious error in supersonic flow is relieved in the Navier-Stokes approach. Furthermore, the approximation of the convective terms in separated flow regions which is necessary for numerical stability in boundary layer calculations is not required in Navier-Stokes calculations. Thus, the basic equations used to solve the interaction problem via a Navier-Stokes calculation are not compromised by approximations which are required for a successful boundary layer solution.

The advantages of the Navier-Stokes solution must be balanced against certain disadvantages such as code complexity, code run time and code storage requirements. Navier-Stokes calculation procedures in general require more code development time than do boundary layer procedures. In addition, Navier-Stokes procedures may require increased computer storage and increased computer run time to obtain a successful solution. A consideration of both the advantages and disadvantages of Navier-Stokes solutions indicate that the potentially increased accuracy of this approach may well balance out the increased requirements in computer storage and run time. With these considerations in mind it seems reasonable to continue development of both approaches to the interaction problem at the present time.

Solutions of the Navier-Stokes equations for shock wave-turbulent boundary layer flow interactions have been presented recently by a variety of authors including Wilcox (Ref. 56), Baldwin and MacCormack (Ref. 2), and Shang and Hankey (Ref. 47). In Ref. 56, Wilcox combined an explicit

first-order finite-difference scheme with Saffman's turbulence model (Ref. 44) to predict two-dimensional turbulent supersonic flows with separation. Although Wilcox was successful in obtaining flow field solutions, the predicted surface pressure distribution disagreed significantly with experimental data. In a more recent work, Baldwin and MacCormack (Ref. 2) applied MacCormack's two-step second-order explicit Navier-Stokes method to the shock wave-turbulent boundary layer interaction problem. Although both a mixing length turbulence model and a two-equation transport model of turbulence were used, neither turbulence model produced flow fields that agreed well with measurements. Shang and Hankey applied the explicit two-dimensional time-dependent method of MacCormack to the interaction flow field problem using an eddy viscosity model which allowed for a lag in the response of the turbulence to the sudden, severe adverse pressure gradient that is characteristic of strong interacting separating boundary layers. A rate relation was introduced to decay the eddy viscosity exponentially from the value at the start of the interaction toward the local equilibrium value with a time scale correlated to the boundary layer thickness. Utilizing the relaxation model for eddy viscosity, Shang and Hankey obtained predictions of a series of compression corner flows which were in good agreement with the experimental data of Law (Ref. 26). More recently, Shang, Hankey and Law (Ref. 48) have compared predictions for a series of incident shock wave-boundary layer interactions with experimental data. Again, good agreement was obtained between the calculations and the experiment.

The Navier-Stokes solutions discussed in the previous paragraph were all based upon an explicit difference scheme for solving the unsteady form of the governing equations. An initial flow field is assumed and the calculation then proceeds in time until a steady state is reached. However, explicit numerical procedures of this type are subject to one or more stability restrictions on the size of the time step relative to the spatial mesh size. These stability limits usually correspond to the well known Courant-Fredricks-Lewy (CFL) condition and in some schemes to an additional stability condition arising from viscous terms. These stability restrictions can lower computational efficiency by imposing a smaller time step than would be otherwise desirable. Since the restriction becomes more and more stringent as the spatial grid is refined, the restriction can become particularly burdensome in the calculation of a turbulent boundary layer where a very fine mesh near the wall may be required. In contrast to most explicit methods, implicit methods tend to be stable for large time steps and therefore offer the prospect of substantial increases in computational efficiency. When the present work was initiated, no implicit Navier-Stokes procedure for predicting the shock wave-boundary layer interaction flow field had been reported in the open literature and in view of the potential benefits associated with implicit methods, it was decided to apply an

implicit technique to this problem. This application represents a feasibility study to determine if the potential benefits of implicit methods could be realized in an interaction problem. If it appears that substantial benefits could be realized, then future work could be aimed toward developing the implicit interaction solution procedure as a design tool.

Since the initiation of the present work, a technique in which viscous terms are treated implicitly and convective terms are treated explicitly has been presented by MacCormack (Ref. 30). The present Navier-Stokes investigation centers on a fully implicit procedure, the Multi-dimensional Implicit Nonlinear Time-dependent (MINT) technique, developed by Briley and McDonald (Ref. 9). The method has been extended to turbulent flow by Briley, McDonald and Gibeling (Ref. 10) and to flow in combustors by Gibeling, McDonald and Briley (Ref. 18). In the Navier-Stokes portion of the present effort a two-dimensional version of the MINT procedure is applied to the shock wave-boundary layer interaction problem.

The present report covers all work performed under the subject contract and can be divided into two parts. The first portion concerns the boundary layer approach; this represents the major portion of the effort done under the subject contract. Under the boundary layer approach, a well-proven weak interaction boundary layer procedure was modified to allow for strong interaction solutions. The modifications include (i) the incorporation of an outer flow analysis, (ii) the revision of the governing equations to allow for flow in separated regions, and (iii) the revision of the turbulence model. The original weak interaction solution procedure, the modifications made under the current effort, and sample calculations are described in the following sections. The second portion of the report concerns the Navier-Stokes approach. The governing equations and the numerical method are discussed and sample calculations are presented.

SECTION II DISCUSSION

THE BOUNDARY LAYER APPROACH

The basis for the strong interaction boundary layer calculations described in this report is a well-proven weak interaction boundary layer procedure which has been used to compute successfully a wide variety of laminar, transitional, and turbulent boundary layers. A complete, detailed description of the procedure as well as an extensive comparison between predictions and data can be found in Refs. 25, 33, 34 and 46. The present discussion first briefly describes the weak interaction procedure and then proceeds to detail the modifications required for a strong interaction code. These modifications include the incorporation of an outer flow analysis into the calculation, the modification of the equations in the reversed flow region, and the modification of the turbulence model within the separation bubble. Next, a discussion of the cause and characteristics of the so-called branching solutions obtained with the strong interaction code is presented. The validity of the branching solutions along with the characteristics of free interactions are presented and the behavior of the branches after encountering a corner or an incident shock wave are demonstrated. Next, attention is focused upon the downstream boundary condition problem. The boundary layer calculation approach used to solve the strong interaction problem requires the downstream boundary conditions to be satisfied through an iterative 'shooting' procedure. In this iterative procedure a sequence of initial value problems is solved until the solution at the end of the strong interaction region is compatible with specified downstream boundary conditions. The initial value problems within the sequence differ in the value of a free parameter. Different values of the free parameter lead to different branching solutions and ultimately to different flow fields at the downstream flow field boundary. The choice of the free parameter is discussed and the rationale for using one variable for the parameter when the solution is far from convergence and another variable for the parameter when the solution is near convergence is presented. Finally, the results of applying the methodology outlined above are presented. Both laminar and turbulent results are presented along with the details of the modified turbulence model that was used in the successful turbulent strong interaction calculations.

Weak Interaction Boundary Layer Procedure

The weak interaction solution, upon which the current work is based, has been developed over a period of years and details of the procedure are presented in Refs. 25, 33, 34 and 46. The procedure itself solves the steady state boundary layer equations for laminar, transitional, and turbulent flow. As shown by many authors (for example, Schubauer and Tchen (Ref. 45)), for two-dimensional or axisymmetric flows, steady in the mean, the boundary layer approximations to the momentum, energy, and continuity equation become:

$$\bar{\rho} \bar{u} \frac{\partial \bar{u}}{\partial x} + \bar{\rho} \bar{v} \frac{\partial \bar{u}}{\partial y} = - \frac{\partial \bar{P}}{\partial x} + \frac{\partial \tau}{\partial y} \quad (1)$$

$$\bar{\rho} \bar{u} C_p \frac{\partial \bar{T}^o}{\partial x} + \bar{\rho} \bar{v} C_p \frac{\partial \bar{T}^o}{\partial y} = \frac{\partial}{\partial y} (Q + \bar{u} \tau) \quad (2)$$

$$\frac{\partial \bar{\rho} \bar{u} r^\alpha}{\partial x} + \frac{\partial \bar{\rho} \bar{v} r^\alpha}{\partial y} = 0 \quad (3)$$

In Eqs. (1) through (3) x and y are coordinates in the streamwise and transverse directions, u and v are velocity components in the x and y directions, ρ is density, P is pressure, C_p is specific heat, T^o is total temperature, r is the radius of curvature for an axisymmetric body, and the exponent α is zero for two-dimensional flows and unity for axisymmetric flows. By definition, the effective shear stress, τ , and the effective heat transfer, Q are given as:

$$\tau = \bar{\mu} \frac{\partial \bar{u}}{\partial y} - \bar{\rho} \overline{u'v'} \quad (4)$$

$$Q = \bar{k} \frac{\partial \bar{T}}{\partial y} - \bar{\rho} C_p \overline{v'T'} \quad (5)$$

where ν is viscosity, k is thermal conductivity, T is static temperature. In Eqs. (1) through (5) overbars indicate averaged quantities and primes indicate fluctuating quantities. The equations are valid for laminar, transitional, or turbulent flows; obviously, for laminar flows the primed quantities are zero. In the case of turbulent and transitional boundary layers, it is convenient to represent the contribution of the apparent turbulent stress, τ_T , to the total shear stress, τ , by an effective turbulent viscosity, ν_T . In an analogous manner, the turbulent contribution to the total heat flux, Q is represented by an effective turbulent conductivity, k_T , such that

$$\bar{\rho} \nu_T \frac{\partial \bar{u}}{\partial y} = - \bar{\rho} \overline{u'v'} \quad (6)$$

$$k_T \frac{\partial \bar{T}}{\partial y} = - \bar{\rho} C_p \overline{v'T'} \quad (7)$$

and by analogy to laminar flow a turbulent Prandtl number, Pr_T , can be defined as

$$Pr_T = \bar{\rho} C_p \nu_T / k_T \quad (8)$$

At this point, ν_T and k_T simply represent definitions and in no way limit the subsequent turbulence modeling. When Eqs. (4) through (7) are substituted into Eqs. (1) and (2), the resulting boundary layer momentum and energy equations take the form:

$$\bar{\rho} \bar{u} \frac{\partial \bar{u}}{\partial x} + \bar{\rho} \bar{v} \frac{\partial \bar{u}}{\partial y} = - \frac{\partial \bar{P}}{\partial x} + \frac{\partial}{\partial y} \left\{ (\bar{\mu} + \bar{\rho} \nu_T) \frac{\partial \bar{u}}{\partial y} \right\} \quad (9)$$

$$\begin{aligned} \bar{\rho} \bar{u} c_p \frac{\partial \bar{T}^0}{\partial x} + \bar{\rho} \bar{v} c_p \frac{\partial \bar{T}^0}{\partial y} &= \frac{\partial}{\partial y} \left\{ \left(\frac{\bar{\mu}}{Pr} + \frac{\bar{\rho} \nu_T}{Pr_T} \right) c_p \frac{\partial \bar{T}^0}{\partial y} \right\} \\ &+ \frac{\partial}{\partial y} \left\{ \left[\left(1 - \frac{1}{Pr} \right) \bar{\mu} + \left(1 - \frac{1}{Pr_T} \right) \bar{\rho} \nu_T \right] \bar{u} \frac{\partial \bar{u}}{\partial y} \right\} \end{aligned} \quad (10)$$

In deriving Eq. (10) use has been made of the definition of total temperature

$$T^0 = T + \frac{u^2}{2C_p} \quad (11)$$

In situations in which the flow is laminar, Eqs. (3), (9), and (10) are solved with $\nu_T = 0$ to determine the boundary layer development. When the flow is transitional or turbulent, it is necessary to model ν_T and Pr_T . The specification of the turbulent viscosity, ν_T , and the turbulent Prandtl number, Pr_T is carried out through the turbulence model described in detail subsequently.

In the present procedure the equations are solved by using the continuity equation to eliminate the explicit appearance of $\bar{\rho} \bar{v}$ from the momentum and energy equations. Then in the weak interaction case where the streamwise pressure gradient, $P(x)$ is specified, the momentum and energy equations, in conjunction with an equation of state and equations governing ν_T and Pr_T , form a closed set of nonlinear, parabolic, partial differential equations which can be solved upon specification of boundary conditions. Obviously, in the strong interaction case where the streamwise pressure gradient, $P(x)$ is not specified a priori but must emerge from the solution, an additional relation is required to determine the static pressure distribution.

The wall and free-stream boundary conditions employed in the solution are given by:

$$\bar{\rho} \bar{v} = (\bar{\rho} \bar{v})_w, u = 0, \bar{T}^0 = T_w \text{ or } \frac{\partial \bar{T}}{\partial y} = 0 \quad (12)$$

at the free-stream, $y \longrightarrow \infty$

$$\bar{\rho} \bar{u} = \rho_e u_e \quad (13)$$

$$\bar{T}^0 = T_e^0$$

The subscripts 'w' and 'e' denote wall and free-stream conditions, respectively. The initial conditions for the problem are set by specifying the initial boundary layer displacement thickness, δ^* , and assuming the initial development is similar in the dimensionless coordinate, η , where

$$\eta = \frac{y}{\delta^*} \quad (14)$$

The numerical procedure used to solve the governing momentum and energy equations is a Hartree-Womersley approach in which streamwise derivatives are replaced by finite differences, the coordinate normal to the wall is nondimensionalized, and a stream function introduced. The resulting momentum equation is a third order nonlinear ordinary differential equation in the transverse coordinate and the energy equation is a second order nonlinear ordinary differential equation in the same transverse coordinate. At each streamwise station the nonlinear coefficients of each equation are estimated from the solution at the previous station and the resulting linearized equations solved as two-point boundary value problems. Appendix A describes the solution procedure in detail.

The fully-developed turbulence model used in the weak interaction procedure was originally presented by McDonald and Camarata (Ref. 32) for two-dimensional incompressible flow and has been extended to a variety of flow situations in Refs. 25, 33, 34 and 46. The model is based upon a solution of the turbulence kinetic energy equation which is a conservation equation derived from the Navier-Stokes equations by writing the instantaneous quantities as a sum of mean and fluctuating parts. The i th Navier-Stokes momentum conservation equation ($i = 1, 2, 3$, referring to the three coordinate directions) is multiplied by the i th component of fluctuation velocity and the average of the resulting three equations is taken. The three averaged equations are summed to obtain the turbulence kinetic energy equation. The derivation of the turbulence kinetic energy equation has been given by Favre (Ref. 17) for compressible flow and approximated by Bradshaw and Ferris (Ref. 8) to boundary layer flows. Two turbulence models are used in the current strong interaction calculations; the first model is a modification of a Prandtl mixing length equilibrium turbulence model. The second model is a modification of the turbulence kinetic energy model presented in Refs. 25, 33, 34 and 46. The modifications are discussed subsequently.

Modifications For Strong Interaction

Matching and Marching Procedures

Although the weak interaction boundary layer procedure described above has successfully predicted the development of a wide variety of boundary layers, it obviously requires as input a specified pressure distribution, $P(x)$. In weak interaction flows the pressure gradient can be obtained from an inviscid

calculation which ignores all viscous displacement effects. However, in strong interaction problems, such as the shock wave boundary layer interaction, the inviscid pressure distribution will be in significant error as the pressure distribution and boundary layer development mutually affect each other. The prediction of the boundary layer development and the pressure distribution using a procedure which recognizes their mutual effects upon each other is the core of the basic strong interaction problem.

The present effort follows the strong interaction approaches of Refs. 14, 21, 24, 27 and 41 which introduce the additional condition that the boundary layer flow angle must agree with the inviscid flow angle at some specified flow location. This condition gives rise to an additional equation which allows the simultaneous prediction of the boundary layer development and the streamwise static pressure distribution. From a straight-forward application of the continuity equation, it can be shown that within the boundary layer the flow angle, θ , at a distance η from the wall is given by

$$\tan \theta = \frac{d\delta^*}{dx} - \frac{(\eta - \delta^*)}{\rho_e U_e} \frac{d\rho_e U_e}{dx} + \alpha \quad (15)$$

where δ^* the displacement thickness, ρ_e the edge (wake) density, U_e the edge (wake) velocity, α the wall angle, and x is the principal flow direction. Using Eq. (15) the inner and outer flows can be matched anywhere between the wall and the boundary layer edge; however, by matching at the displacement surface ($\eta = \delta^*$), the second term on the right-hand side of Eq. (15) becomes identically zero and the resulting expression becomes

$$\tan \theta = \frac{d\delta^*}{dx} + \alpha \quad (16)$$

As can be seen from Eq. (15), the choice of location at which the flows are to be matched is somewhat arbitrary. Two locations which have been used commonly are the boundary layer edge, δ , and the displacement surface, δ^* . For relatively thick boundary layers, either choice represents a compromise. If δ matching is chosen, the entire viscous region is included below the matching line; however, the region below the matching line also includes a region of transverse pressure gradients which are ignored in the boundary layer calculation. When δ^* -matching is used, the region below the matching line is expected to contain negligible transverse pressure gradients; however, significant viscous and rotational effects may be present above the matching line. In the present effort δ^* -matching was used.

The boundary layer equations are solved by a forward marching procedure in which the inner and outer flows are coupled at each step. The procedure is an iterative one which first approximates the displacement thickness (or edge flow angle from Eq. (16)) through an extrapolation of the solution at previous stations. The boundary layer momentum equation then is solved using the specified displacement thickness to obtain both the boundary layer flow field and the edge flow conditions. Thus, for an assumed flow angle, the viscous calculation predicts a certain edge velocity. Using an outer inviscid flow relation and the boundary layer edge velocity, this flow angle is determined again and the two values of the flow angle are compared. If the two flow angles agree within a tolerance, the outer and inner flows are considered to be matched. If not, a new displacement thickness is assumed and the procedure repeated. The modifications in the equations which allow specification of δ^* for the boundary layer solution are presented in Appendix B.

After the momentum equation is matched with the outer flow law, the energy equation is solved. The velocity, density, and temperature field are then evaluated. The matching procedure is repeated at each streamwise step and thus, a solution is produced by marching in the streamwise direction.

Outer Flow Analysis

As discussed above, the strong interaction procedure requires an inviscid flow law which gives a unique relation between the flow angles and velocity. In the present study, the well-known Prandtl-Meyer relationship for flows with waves of one family was used to describe the outer flow. Under the Prandtl-Meyer relationship, the flow angle, ω , and the Mach number, M , are related by

$$\omega = \sqrt{\frac{\gamma+1}{\gamma-1}} \tan^{-1} \sqrt{\frac{\gamma-1}{\gamma+1} (M^2 - 1)} - \tan^{-1} \sqrt{M^2 - 1} \quad (17)$$

where γ is the ratio of specific heats. At hypersonic Mach numbers the tangent-wedge relation can readily be substituted for the Prandtl-Meyer relation and, in fact, if desired, the viscous procedure can be coupled to a supersonic inviscid flow code to predict as much of the outer flow field as desired.

Separated Flow

Since the boundary layer equations are solved by a forward marching procedure, numerical instabilities are expected to be generated in the reverse flow region when the reverse velocities are large or when the reverse flow region extends over a large portion of the flow. As shown by several authors (e.g., Ref. 41), the source of this instability is in the streamwise convective terms. In the present effort, the instability is suppressed by the usual

method of approximating the convective terms in the reversed flow region. In so far as the energy equation is concerned, the streamwise convective term was simply neglected in regions of reversed flow. Since the present solution of the boundary layer equations is based upon a stream function formulation, the suppression of the convective instabilities in the momentum equation may not be obvious and, therefore, the suppression of this term in the momentum equation is now discussed in some detail.

In the present procedure a stream function formulation is used in which the stream function, F , is of the form:

$$\frac{\partial F}{\partial y} = 1 - \frac{\rho u}{\rho_e u_e} \quad (18)$$

and the transverse velocity v is related to the stream function through application of the continuity equation

$$\frac{\partial \rho u}{\partial x} + \frac{\partial \rho v}{\partial y} = 0 \quad (19)$$

which yields a relation of the form:

$$\rho v = - \frac{\partial \rho_e u_e}{\partial x} (y - F) + \rho_e u_e \frac{\partial F}{\partial x} \quad (20)$$

In Eqs. (18) through (20) x and y are the streamwise and transverse coordinates, u and v are the velocity components in the x and y directions, ρ is the density, and the subscript 'e' indicates the quantity is evaluated at the edge of the boundary layer. After a coordinate transformation of the form

$$x' = x \quad \eta = y/\delta^+ \quad (21)$$

is made, the partial differential equations are reduced to ordinary differential equations by approximating derivatives in the streamwise direction by two point backward differences; i.e., for the variable F ,

$$\frac{\partial F(x, \eta)}{\partial x} = \frac{F(x, \eta) - F(x - \Delta x, \eta)}{\Delta x} \quad (22)$$

As can be seen from the original form of the momentum equation

$$\rho u \frac{\partial u}{\partial x} + \rho v \frac{\partial u}{\partial y} = - \frac{dp}{dx} + \frac{\partial \tau}{\partial y} \quad (23)$$

and an examination of Eq. (20) derivatives of the stream function, F , with respect to the streamwise coordinate x arise both through the terms $\rho u \partial u / \partial x$, which controls streamwise convection and $\rho v \partial u / \partial x$, which controls transverse convection. When contributions of both these terms to $\partial F / \partial x$ were neglected in regions of reversed flow, the solution became unstable. However, when only the contribution of $\rho u \partial u / \partial x$ was neglected in the reversed flow region, a stable solution was obtained. In this latter case the factor $\partial F / \partial x$ which arises from the term $\rho v \partial u / \partial y$ is treated as a nonlinear coefficient whose value was approximated by extrapolation of the stream function from previous stations. This method of approximating the convective terms in the momentum and energy equations rendered the system marginally stable in the presence of reversed flow. However, when calculating turbulent boundary layers with large, high speed reversed flow regions instabilities occurred. Following Reyhner and Flugge-Lotz (Ref. 41), rather than simply neglecting these contributions to the convective terms in the momentum equations, the absolute value of the appropriate coefficients were used to provide added stability.

Turbulence Model

In the early stages of the present work the turbulence model used was identical to that used in the weak interaction solution (See Appendix C). Since this turbulence model was developed for attached flows, the resulting poor agreement for separating flows between calculations and data was not unexpected. The weak interaction turbulence model was based upon a mixing length model in which the mixing length was determined either by an equilibrium turbulence assumption or by the solution of the integral turbulence kinetic energy equation. This turbulence model was well-known and when used in the turbulence kinetic energy mode has been proven accurate for a broad spectrum of attached boundary layer flows (Refs. 25, 33, 34 and 46). In strong interaction separating flows, however, the basic model developed for attached flow yielded poor agreement with data even when used in the turbulence energy mode and, in fact, calculations made with the original model in the turbulence energy mode showed little difference from calculations made with the original equilibrium model. Thus, both models appeared inadequate in separated flows.

In a recent paper (Ref. 40) Owen showed that in the case of confined coaxial jets with recirculation, the turbulence followed the dividing streamline and appeared to diffuse from this streamline as the main flow progressed downstream. Little turbulence was found in the reversed flow region. Based upon some computational turbulence studies and the data of Owen, a modification of the basic turbulence model was postulated for boundary layers containing recirculating flow. The details of the modified turbulence model are presented in the Results section of this report along with comparisons of computations using this modified model and test data.

Solution Of The Strong Interaction Boundary Layer Equations

The strong interaction boundary layer procedure was formed by modifying the existing weak interaction boundary layer code in the manner described previously. However, the application of the forward marching strong interaction procedure to compression corner or incident shock problems requires an iterative method of solution based upon the branching solutions obtained when the interaction is treated as a forward marching problem. Therefore, the present section discusses characteristics of the family of branching solutions that can emerge in strong interaction computations. As will be discussed in detail subsequently, the forward marching procedure can be posed so that the problem contains a free parameter. Different choices of the free parameter lead to different branching solutions and the iterative solution consists of determining what value of the free parameter is required to satisfy specified downstream boundary conditions. Since proper choice of the free parameter produces the desired computational solution, characteristics of the selection and iterative updating of the free parameter also are discussed.

Characteristics of the Branches

The nature of the solution to the strong interaction boundary layer equations has been the subject of a series of investigations (Refs. 5, 19, 22, 24, 27 and 41). In brief these investigations have shown that the strong interaction boundary layer equations can be satisfied by a family of solutions (see Fig. 1) consisting of the classical weak interaction solution (termed the fundamental solution) and in addition, a family of branching or departure solutions (termed free interaction solutions). From a numerical point of view Tyson (Ref. 53) has shown that these branching solutions can emerge in solving finite difference equations when the streamwise step size is chosen to be less than a characteristic departure length; for large streamwise step sizes only the fundamental weak interaction solution emerges. The validity of these branches as eigensolutions of the laminar boundary layer equations was demonstrated by Hankey, Dwoyer, and Werle (Ref. 20) and the role of the initial conditions in determining which branch of the family of solutions emerges was investigated by Werle, Dwoyer, and Hankey (Ref. 54). Both Refs. 20 and 54 demonstrate that a single free parameter exists in the initial conditions to the solution of the laminar strong interaction boundary layer equations that controls which of the many physically possible branching solutions will emerge. By controlling the free parameter one can select the branch to emerge from the solution. More recently Bertke, Werle, and Polak (Ref. 5) have demonstrated that the strong interaction turbulent boundary layer equations contain branching characteristics analogous to the laminar branches described above.

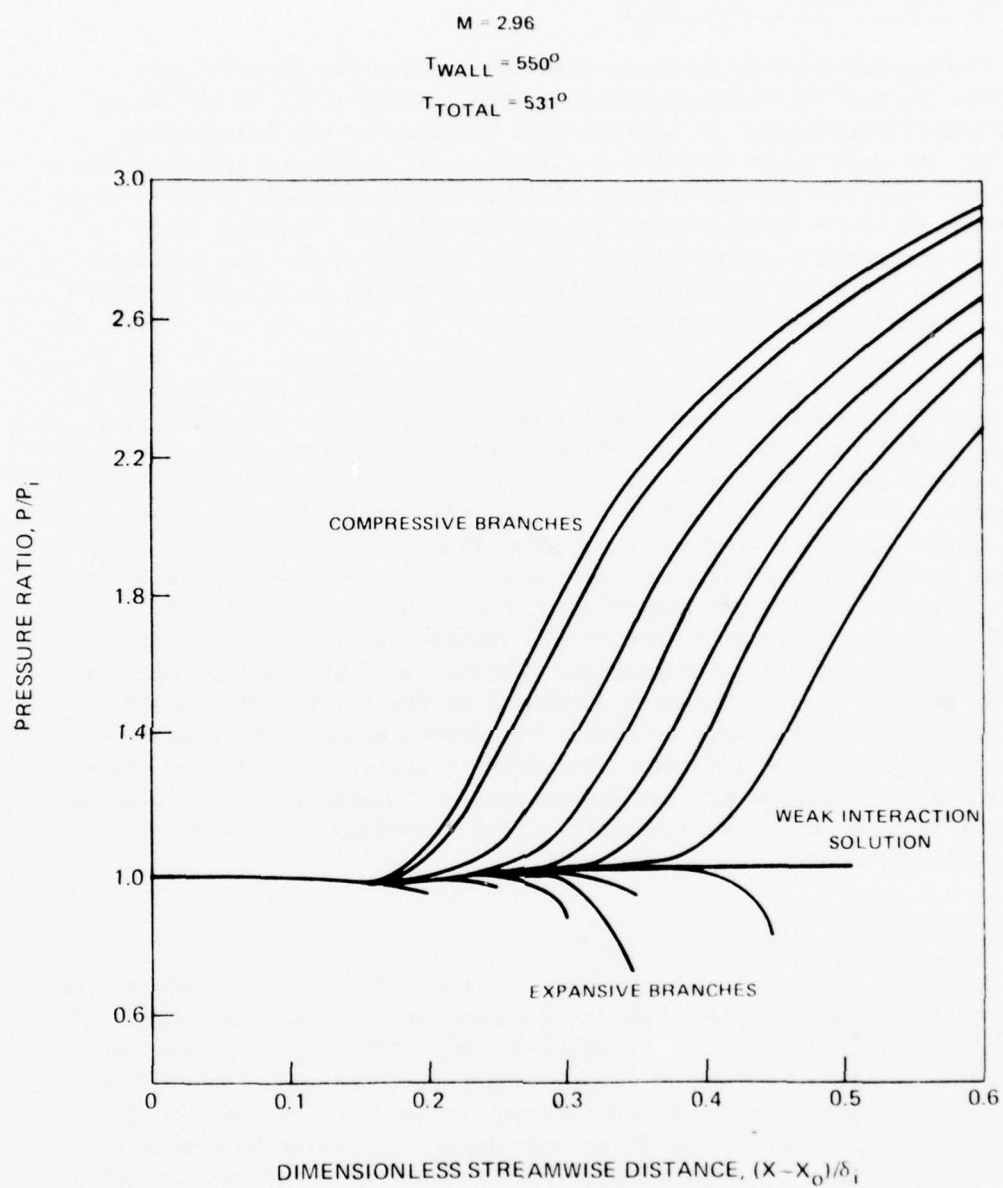


Figure 1. Departure Solutions to the Boundary Layer Equations

Downstream Boundary Conditions

An obvious problem which arises when the interaction flow field is solved via a forward marching procedure is the specification of the downstream boundary condition. At the upstream boundary of the calculation region, the boundary layer velocity and density distributions are specified. At the downstream station the correct boundary condition must be based upon the pressure (or Mach number) being consistent with the incident shock strength or compression corner angle. In the present effort the condition chosen is that the axial pressure gradient be zero when the static pressure is equal to the inviscid downstream value.

Since the strong interaction boundary layer equations are solved by a forward marching technique, an iterative solution procedure is employed to couple the downstream boundary conditions into the solution. First, values of the boundary layer properties as well as the free parameter controlling the branching are set at the upstream boundary of the flow field. The boundary layer equations coupled to an outer flow law are then integrated downstream by the implicit finite difference procedure outlined previously and the pressure distribution generated by the solution is monitored. If the axial pressure gradient is zero at the station where the static pressure is that given by inviscid considerations downstream of the shock, then the problem is solved; if not, the free parameter at the initial station is changed and the boundary layer equations integrated again. The iteration on the free parameter at the initial value plane is continued until the downstream boundary conditions are met to the desired tolerance. This procedure is simply a variant of the well known shooting technique for two-point boundary value problems.

Branch Control

The boundary layer calculations were started using the weak interaction boundary layer procedure to predict the development of a boundary layer under an imposed constant static pressure distribution. After marching several steps to settle out the effect of initial conditions, the weak interaction calculation was replaced by a strong interaction calculation. At the point of switching to the strong interaction calculation the solution branch was selected by imposing a pressure gradient at the last weak interaction station. In general, the stronger the adverse pressure gradient imposed, the sooner the compressive branch emerged. The more favorable the imposed gradient, the later the compressive branch emerged. Even more favorable imposed pressure gradients produce expansive branches. Since the branching behavior is determined by the details of the boundary layer profiles at the start of the interaction (Ref. 54), it was not possible to determine in advance the imposed pressure gradient that would produce a given branch. In general, a series of runs were made for each case to determine empirically the details of the relation between the imposed pressure gradient and the emerging branch solution.

The free parameter that was used to impose the pressure gradient at the start of the strong interaction was a perturbation in the edge velocity termed a "kick". Obviously, the perturbation in edge velocity imposed a specified pressure gradient upon the boundary layer at the last weak interaction station. Although an imposed pressure gradient was used as the "free parameter" in the present study, this was only one of several possible methods which could be used to generate the required series of branching solutions. In the process of iterating on a solution, small changes in the kick at the start of the interaction are required to produce changes in the flow field at the downstream boundary. However, in the process of integrating the strong interaction boundary layer equations downstream, small changes in the initial flow field become smothered by truncation error from the linearizations and from the classical problem of significant figures. One solution to this problem has been to go to double precision on the computer and thereby gain additional significant figures in the calculation.

Another method for controlling the branches was found that obviated the need for double precision. This method consists of dividing the interaction procedure into two parts, each using a different but conceptually equivalent free parameter. First the kick is used as the free parameter that determines the location of the start of the free interaction relative to the location of the incident shock or compression corner. The iteration on the kick, described above, is used until the limit in significant figures was approached. The kick is then frozen at the latest value. The second part of the iteration uses the distance between the start of the free interaction and the location of the incident shock or compression corner as the free parameter. Leaving the upstream solution unchanged, the location of the shock or corner is moved up or downstream until the downstream flow field is compatible with the downstream boundary conditions. The change in free parameter used to control the iteration has removed the need for double precision in the cases that were investigated.

Results

The strong interaction boundary layer was computed by iteratively selecting compressive branches of the boundary layer equations until compatibility with the downstream boundary conditions was obtained. This section presents the results of applying this strong interaction boundary layer calculation procedure to a series of laminar and turbulent compression corner flows. The laminar runs are presented to verify the procedure used since the laminar calculations are not complicated by turbulence modeling. Both the validity of the numerics and the control of the branching solutions are presented. When turbulent strong interaction calculations were performed, the qualitative behavior of the solutions was found to be the same as in the

laminar case, however originally the quantitative agreement with experimental data was found to be poor. The source of the problem in the case of turbulent flows was found to be the turbulence model. Therefore, based upon some recent experimental data of Owen (Ref. 40) a revised turbulence model was postulated. Turbulent solutions with both the original and the revised model are presented subsequently.

Laminar Flow

Other investigators have achieved apparently accurate predictions of laminar interacting boundary layers using physical assumptions similar to those used in the present effort. These available solutions can be used to confirm the correct operation of the UTRC Code. Furthermore, the laminar case provides a direct confirmation of the numerics since it is not complicated by the turbulence modeling required for turbulent boundary layer calculations.

In separating boundary layers, experimental data (Refs. 11, 13, 16 and 49) indicates that when separation in supersonic flow results from an incident shock or a compression corner, the shape of the initial pressure rise and the associated changes in the boundary layer profile are independent of the specific cause of the compression, a phenomenon termed free interaction. Experimental data also shows that the distance between the start of the pressure rise and the incident shock or compression corner increases as the strength of the imposed compression increases. Thus for given conditions, free interaction pressure distributions form a family of identical initial pressure rise contours (Fig. 2) whose location relative to the location of the incident shock or compression corner is determined by the strength of the overall compression. Two free interaction pressure distributions are parallel to each other only being separated by a constant displacement in the streamwise direction. It should be noted that both laminar and turbulent boundary layers have been found experimentally to exhibit this free interaction property. In the case of laminar flow the various pressure rise curves reach a common plateau at a pressure level termed the "plateau pressure" (see Fig. 2) which occurs at a streamwise location upstream of the incident shock or compression corner.

In the present effort in which strong interacting boundary layers are computed by a forward marching procedure, departure solutions emerge and, as described in the previous section, these computational branching solutions are bona fide solutions of the boundary layer equations. The behavior of these computational branching solutions was found to correspond in a qualitative manner to the experimentally observed free interactions for both laminar and turbulent separating boundary layers. For given flow properties different departure solutions give pressure rises which initially are parallel and only differ in the location of the pressure rise. The computed laminar branching

DATA OF CHAPMAN ET. AL (REF. 11)

$M_n = 2.0$

10^0 RAMP

○ $Re_C = 0.18 \times 10^6$

◇ $Re_C = 0.42 \times 10^6$

△ $Re_C = 1.26 \times 10^6$

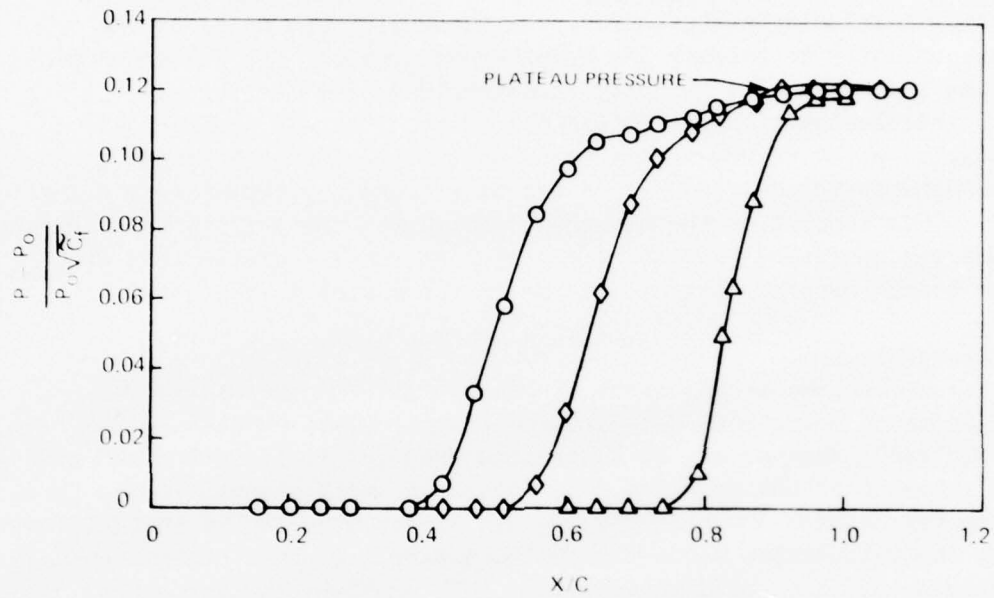


Figure 2. Experimental Free Interaction Pressure Rise

solutions obtained in the present study were compared to the free interacting plateau pressure correlation of Curle (Ref. 14) and the pressure rise to separation correlation of Chapman, et al (Ref. 11) in Fig. 3. The comparisons of the calculations with the data correlations show the predictions of the present procedure to be in good agreement with both the separation pressure and the plateau pressure correlations.

Two calculations corresponding to two different upstream conditions are shown in Fig. 3. In both calculations the interacting solutions are started by first marching the code for several streamwise stations under a specified free-stream velocity distribution, i.e., an imposed pressure distribution. A velocity perturbation, the "kick", is then added to the imposed edge velocity to trigger the branching solutions. At stations downstream of the kick, the edge velocity is determined from the strong-interaction calculation. Different kicks lead to different profiles at the last station prior to the interaction and thus lead to different solution branches. The desired branch can be selected by iteratively changing the "kick". This control of the branches, along with the ability to calculate reattachment was confirmed by running a series of sample calculations at $M = 4$. The branch control obtained via an upstream kick is presented in Fig. 4.

When the conditions at the start of the interaction are varied in an attempt to match downstream boundary conditions, small changes in the kick are required. Because of the tolerances used in the iteration and the truncation inherent in the solution, the effect of small changes in the "kick", smaller than the changes shown in Fig. 4, can become numerically insignificant by the time the calculation marches past the corner. Tighter tolerances and double precision could be used to alleviate this problem, however either of these would have an associated increase in computer run times. Therefore, a second method of branch control was investigated in order to control the reattachment and downstream branching. The second method of control was obtained by displacing the compression corner small distances up or downstream relative to the start of the interaction. Control of the reattachment and downstream branching solutions was successfully obtained by this means as shown in Fig. 5. In practice a combination of both methods of branch control is employed. The "kick" in edge velocity at the start of the interaction is used to control the branching until the downstream solution became insensitive to small changes in the "kick". Final resolution of the downstream boundary condition is accomplished by small displacements of the location of the compression corner. Applying this two stage method of branch control, a laminar strong interaction calculation was made to compare to the data of Lewis, Kubota, and Lees (Fig. 6). After a suitable kick was imposed, various branching solutions were obtained by corner displacement. As expected, two

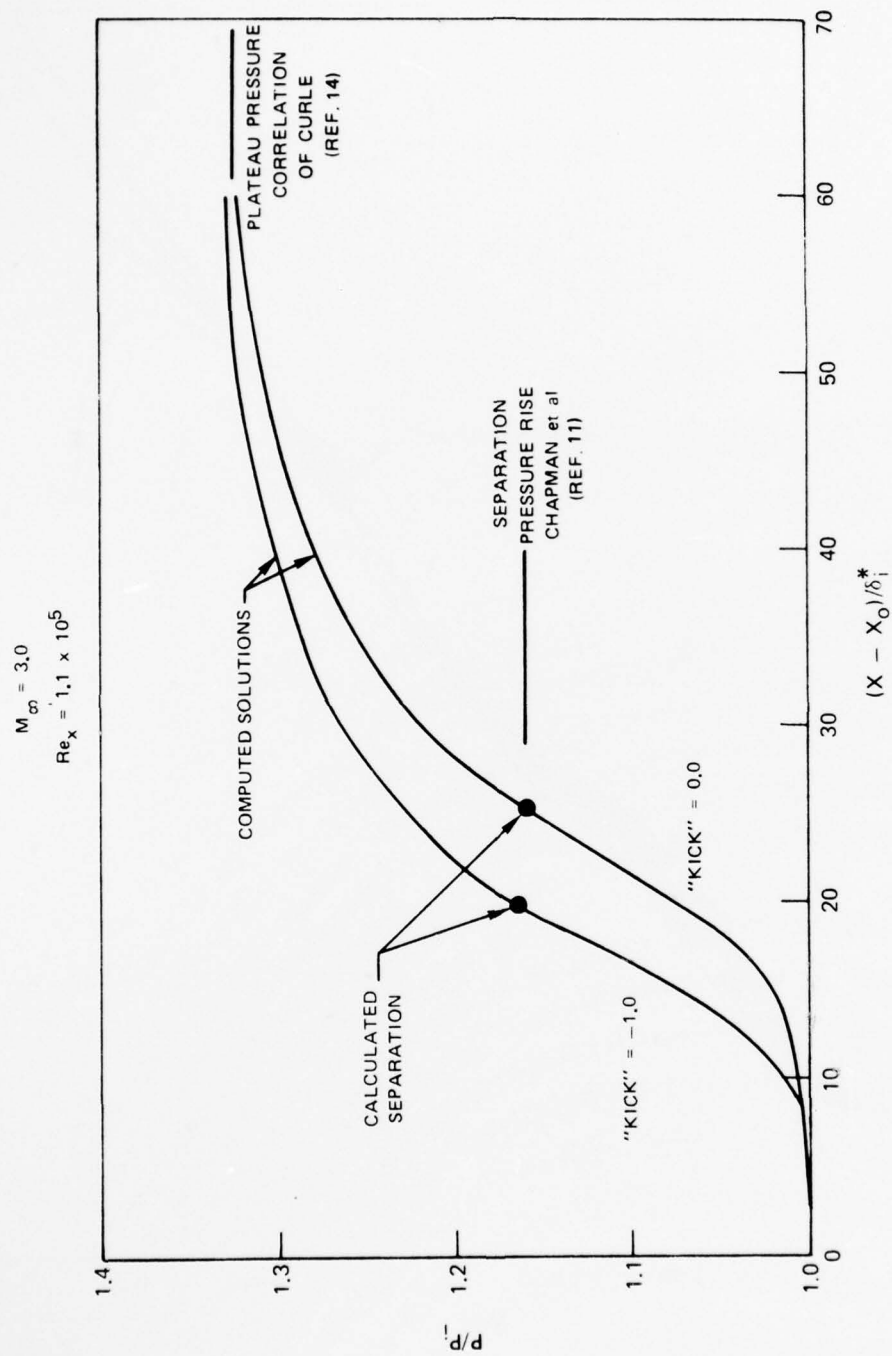


Figure 3. Laminar Free Interaction Calculations

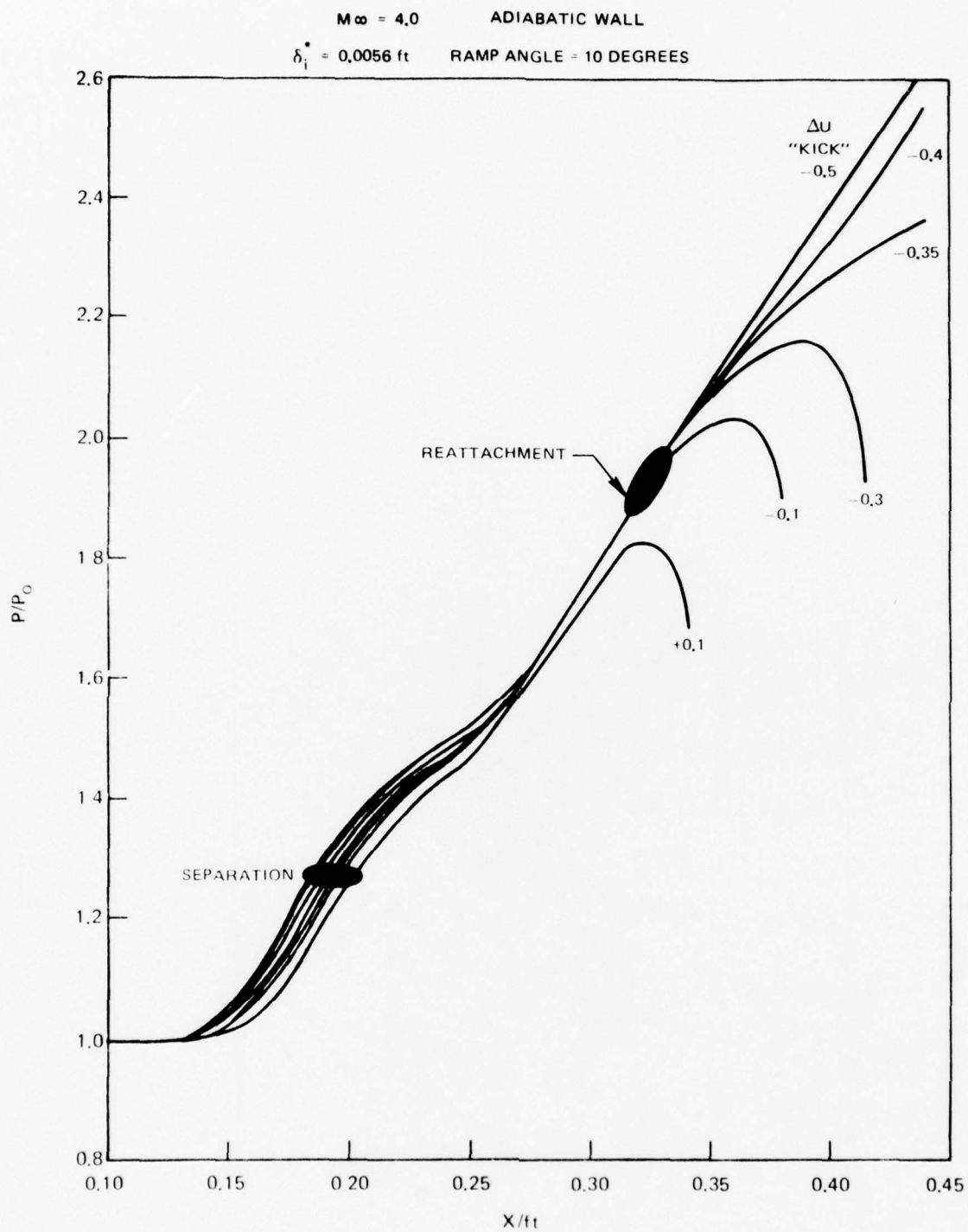


Figure 4. Laminar Calculation Branch Control Using Kick

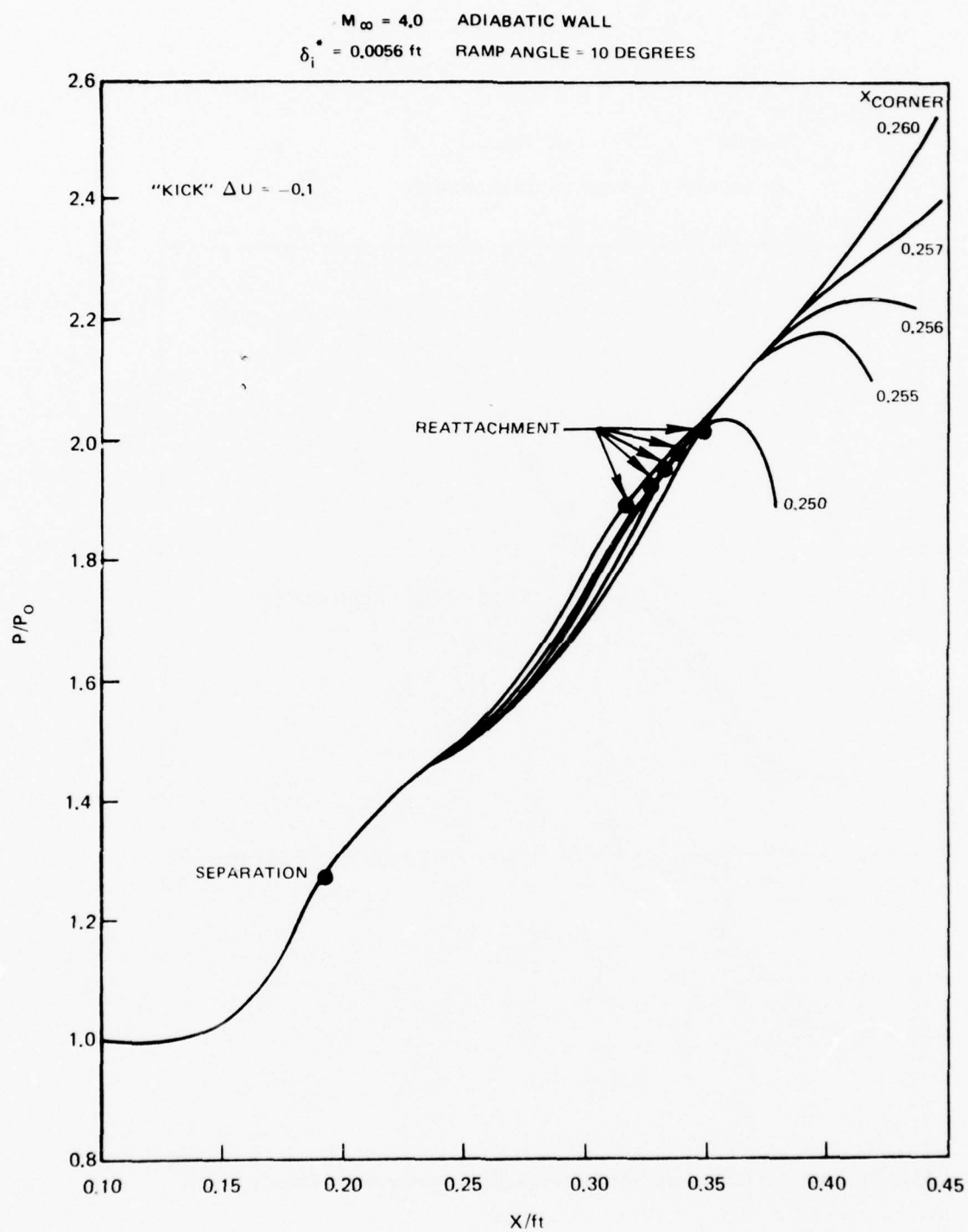


Figure 5. Laminar Calculation Branch Control Using X_{corner}

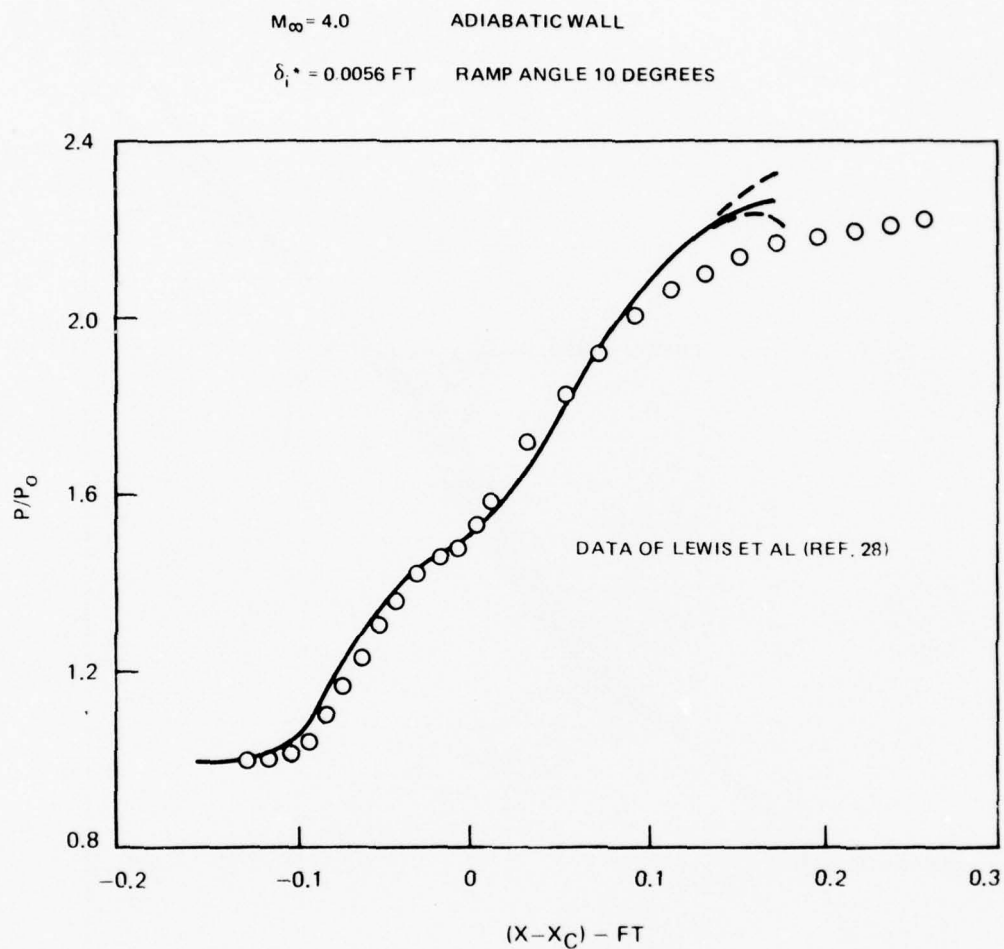


Figure 6. Laminar Strong Interaction Flow Over Compression Corner

families of solutions emerged: one giving continually increasing pressure and one giving a pressure maximum followed by a pressure decrease. Since this study is primarily concerned with strong interacting turbulent boundary layers, the pressure overshoot that occurs in laminar boundary layers after reattachment (Ref. 28) is not addressed in this report. The corner location was iterated upon to move the branching location between the two families further and further downstream. The results of the calculation are presented in Fig. 6 which shows good agreement with data over most of the interesting range.

Turbulent Flow

After the procedure was confirmed through the laminar calculations presented in Figs. 3-6 the procedure was applied to strong interacting turbulent boundary layers. The results appeared to be qualitatively reasonable, however, the free interaction pressure rise was more abrupt and led to higher plateau pressure than was indicated by data as shown in Fig. 7. Similar results were obtained by Bertke, Werle, and Polak (Ref. 5) using a different turbulence model. In the present code the computed turbulence structure is based upon a mixing length model in which the mixing length can be determined by either an equilibrium turbulence assumption (equilibrium model) or by the solution of the integral turbulence kinetic energy equation (TKE model). Under either the equilibrium or TKE option, the turbulence structure is based upon an assumed one-parameter mixing length profile which varies with distance from the wall as a hyperbolic tangent function. In the immediate vicinity of the wall the mixing length is damped by a probability damping function. The free parameter in the profile is the "wake" value of the mixing length; i.e., the value far removed from the wall. When the equilibrium turbulence option is used, this wake value is a function of the boundary layer thickness and the local momentum thickness Reynolds number. When the turbulence kinetic energy option is used, the "wake" value of the mixing length emerges from the solution of the integral turbulence kinetic energy equation.

A turbulent free interaction was computed first with the equilibrium model and then with the TKE model. As shown in Fig. 8, the calculated wall pressure and skin friction distributions were found to be virtually identical even though the wake mixing length distributions of the two methods differed considerably (see Fig. 9). The low Reynolds number correction factor (Appendix C) is used in both cases. In an attempt to gain some insight into the sensitivity of the wall pressure distribution to the turbulence modeling assumptions a series of frozen turbulence models were evaluated. First, the eddy velocity was frozen at the value at the start of the interaction and held constant along lines of constant distance from the wall ($y = \text{const}$). Second, the turbulence intensity (Reynolds shear stress $-\overline{u'v'}$) was frozen at the start of the interaction and again held constant along $y = \text{const}$.

$M_\infty = 2.93$
 $Re = 3.63 \times 10^4$

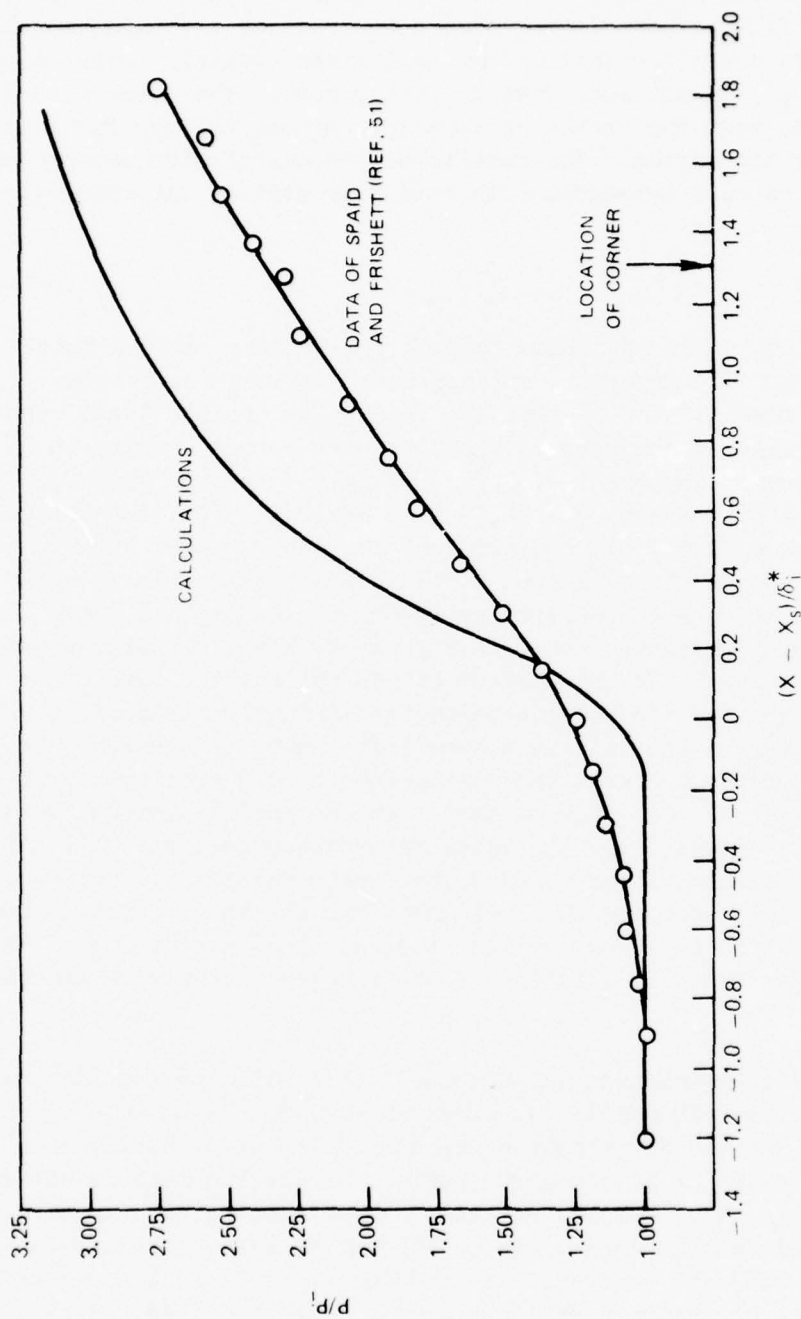


Figure 7. Separating Turbulent Strong Interaction Solution Using Weak Interaction Turbulence Modeling Assumptions

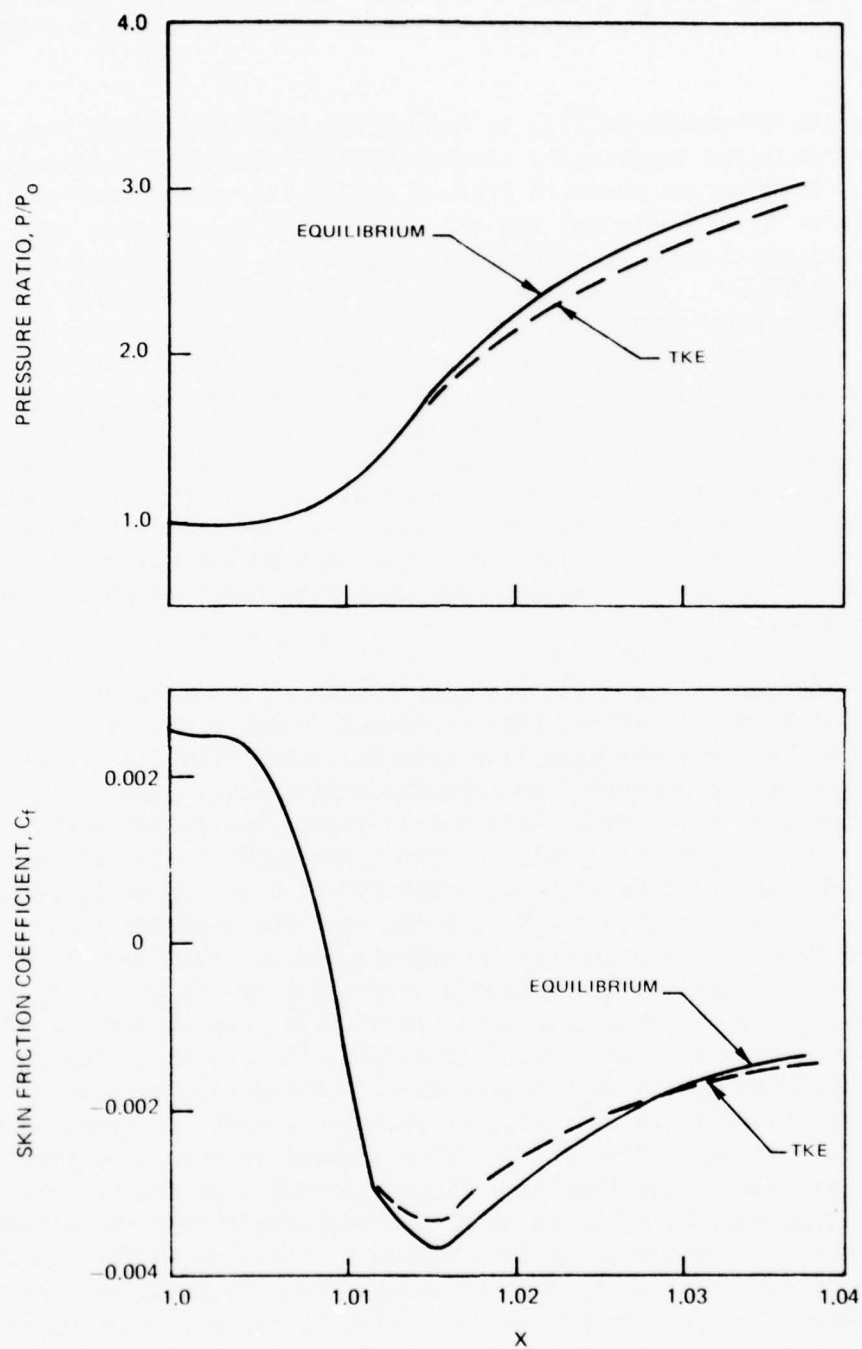


Figure 8. Comparison of Equilibrium and TKE Options for Attached Boundary Layer Turbulence Model

Third, the eddy viscosity was frozen and held constant along streamlines, and fourth, the turbulence intensity was frozen and held constant along streamlines.

The results presented in Fig. 10 demonstrate that the wall pressure distributions could be drastically altered by the turbulence modeling assumptions. However, as shown in Figs. 9 and 10 the wall pressure distributions produced by the original TKE and equilibrium models were very similar yet the wake mixing length distributions produced by these assumptions were considerably different. To resolve this apparent contradiction an investigation was made into the details of the turbulence structure produced by the TKE and equilibrium models. The mixing length distributions within the boundary layer produced by the TKE and equilibrium models were compared as shown in Fig. 11 at three streamwise locations. Although the TKE and equilibrium models produce significantly different values of the wake mixing length, Fig. 11 shows that the turbulence modeling near the wall remains unaffected by the changes in the wake turbulence. Thus the problem with the turbulence modeling may not be one of predicting the wake properties but may be one of predicting the distribution of turbulence near the wall, especially in the recirculating region.

In a recent paper (Ref. 40) Owen showed that in the case of confined coaxial jets with recirculation, the turbulence followed the dividing streamline separating the recirculating flow from the outer flow (in a time averaged sense) and appeared to diffuse from this streamline toward the wall as the main flow progressed downstream. Little turbulence was found in the reversed flow region. Based upon the results of the turbulence studies presented in Figs. 9-11 and upon the data of Owen, a modification of the basic turbulence model in the near wall region has been postulated for boundary layers containing recirculating flow. This modification employs the observation that in attached boundary layers the wall is a continuous streamline of the flow. In separated boundary layers, the dividing streamline is the limiting streamline of the main flow region, and the turbulence approaching the recirculation region is convected around the bubble by the mean flow. Therefore, the damping of the turbulence from the wall in the original turbulence model is replaced by damping of the turbulence from the dividing streamline when a recirculation is present. Since Owen's data implies a slight spreading of the turbulence into the recirculating region, a diffusion of the turbulence from the dividing streamline into the recirculating flow region is included in the modified model. This diffusion is postulated to spread the turbulence at a 40° half angle into the forward flow portion of the recirculating region. Damping by the wall is expected to have a strong effect in the relatively low speed reversed flow, and since Owen found little turbulence in this region the turbulence is assumed to be completely damped in the reversed flow. In attached boundary layers, the modified turbulence model collapses into the original model. Mikulla and

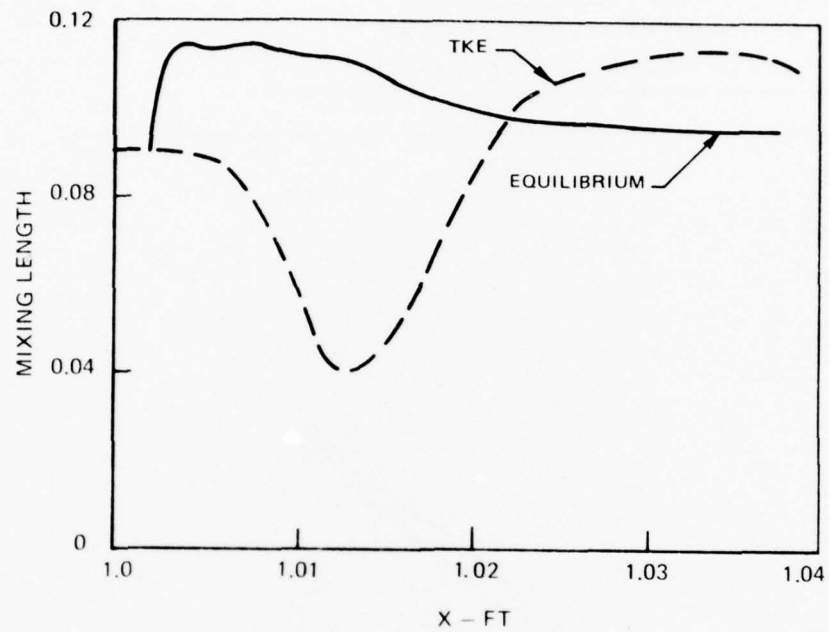


Figure 9. Wake Mixing Length Distribution With Attached Boundary Layer Turbulence Model Including Low Reynolds Number Correction

CURVE	THEORY
1	EQUILIBRIUM TURBULENCE
2	TURBULENCE KINETIC ENERGY EQUATION
3	FROZEN VISCOSITY ALONG $Y = \text{CONST.}$
4	FROZEN TURBULENCE ALONG $Y = \text{CONST.}$
5	FROZEN VISCOSITY ALONG S.L.
6	FROZEN TURBULENCE ALONG S.L.
DATA OF SPAID AND FRISHETT (REF. 51)	

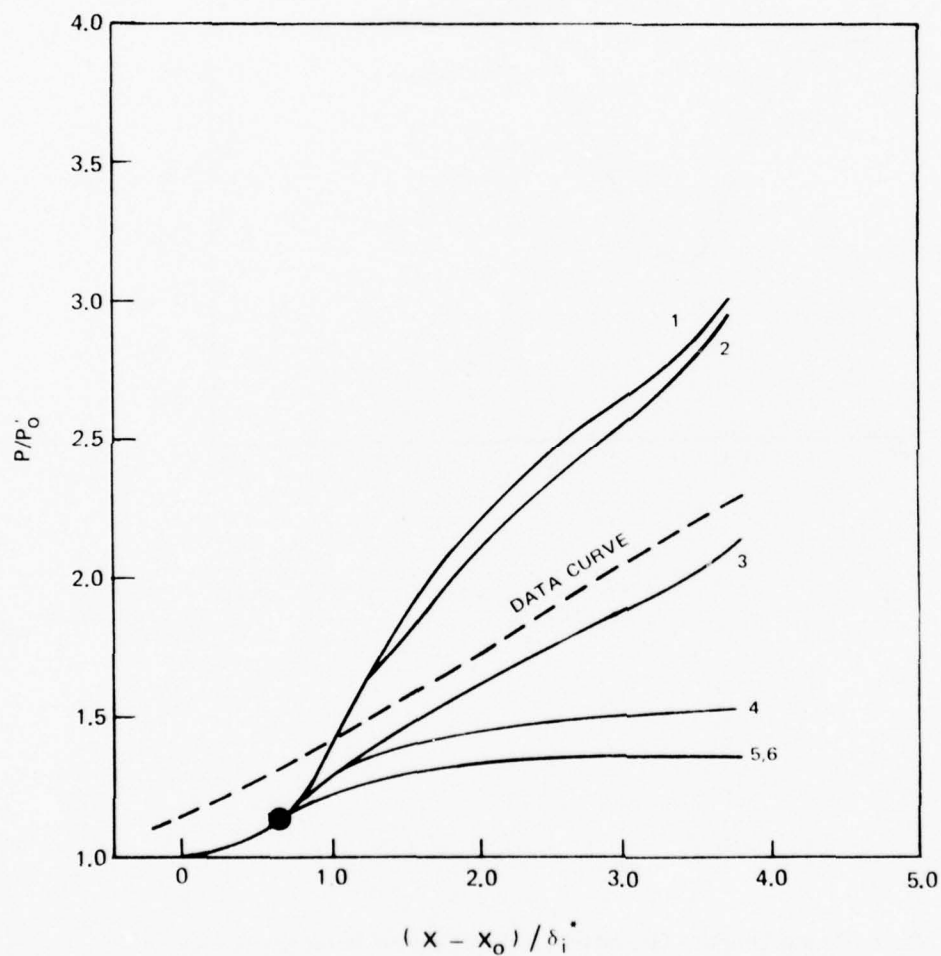


Figure 10. Sensitivity of Free Interactions to Turbulence Assumptions

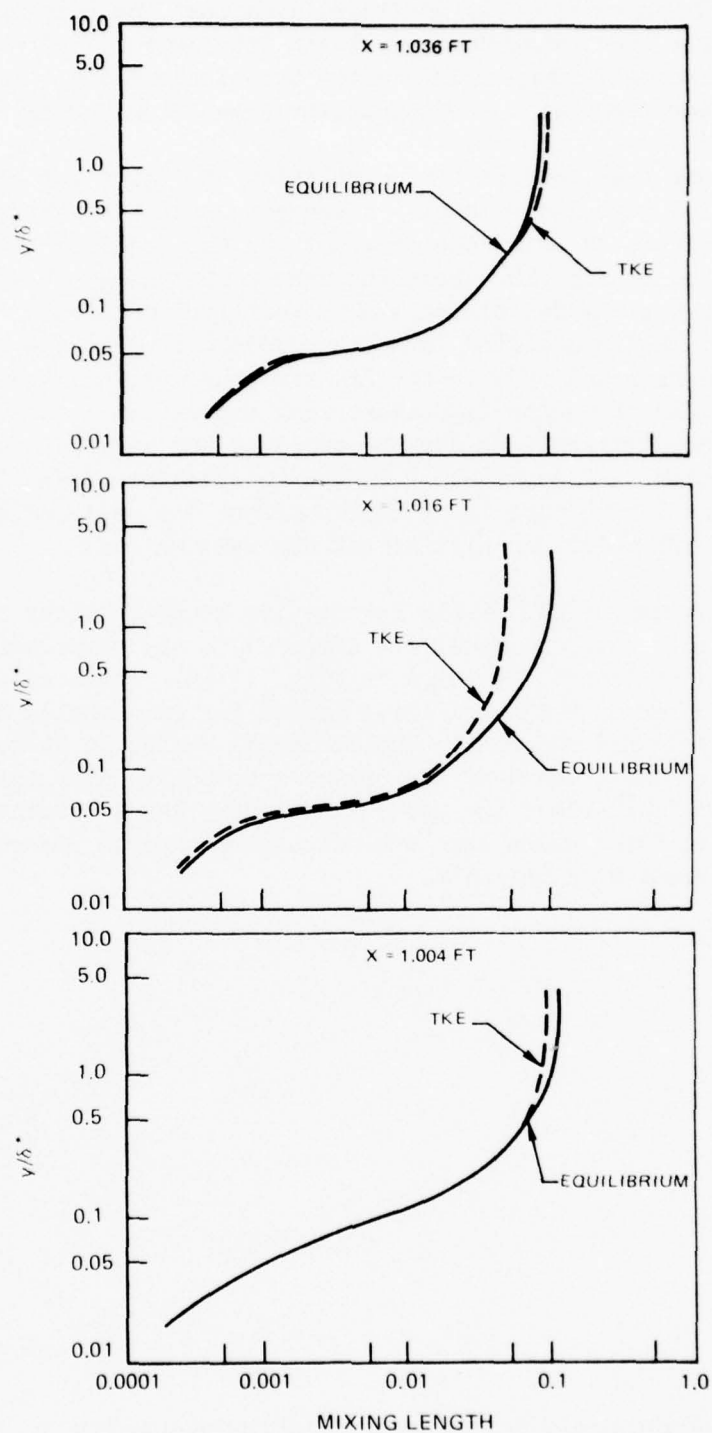


Figure 11. Normal Mixing Length Distributions With Attached Boundary Layer Turbulence Model

Horstman (Ref. 36) have recently published data that includes turbulence measurements for a shock wave-boundary layer interaction. Although the measurements taken only roughly define the turbulence field, the data is in qualitative agreement with the conclusion drawn from the data of Ref. 40.

The turbulent free interaction calculation of Fig. 7 was recalculated using the modified turbulence model. A comparison of the wall pressure distributions calculated using the original and the modified turbulence model is presented in Fig. 12, where the wake mixing length has been set in both cases by the Prandtl mixing length equilibrium turbulence model. As shown in Fig. 12 the modified turbulence model corrects the overly abrupt initial pressure rise and reduces the plateau pressure, and therefore, the modified model leads to better agreement with experimental data. A comparison of the turbulence distributions for the original and modified turbulence models is presented in Figs. 13-16. It can be seen from Figs. 13-16 that the modifications in the turbulence models affect the wall region and in the case of the TKE model can also affect the wake region.

The calculations of the strong interaction boundary layer procedure with the modified turbulence model are compared to the compression corner data of Spaid and Frichett (Ref. 51) in Figs. 17-19. Three cases at an upstream Mach number of 2.93 were investigated for ramp angles of 9.81° , 16.06° and 19.67° . The separation bubble length varies in these cases from very small, less than a third of the upstream boundary layer thickness, to very large, over $2\frac{1}{2}$ times the upstream boundary layer thickness. Figures 17-19 show in all three cases that the calculated overall pressure distribution is in good agreement with the data.

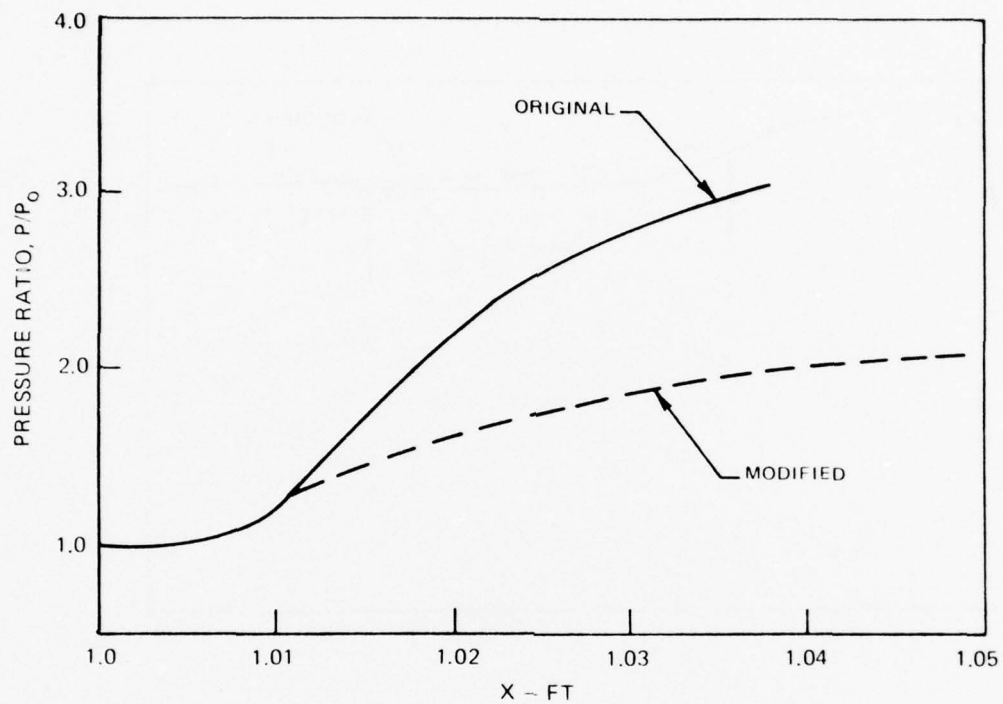


Figure 12. Free Interaction Wall Pressure Distributions

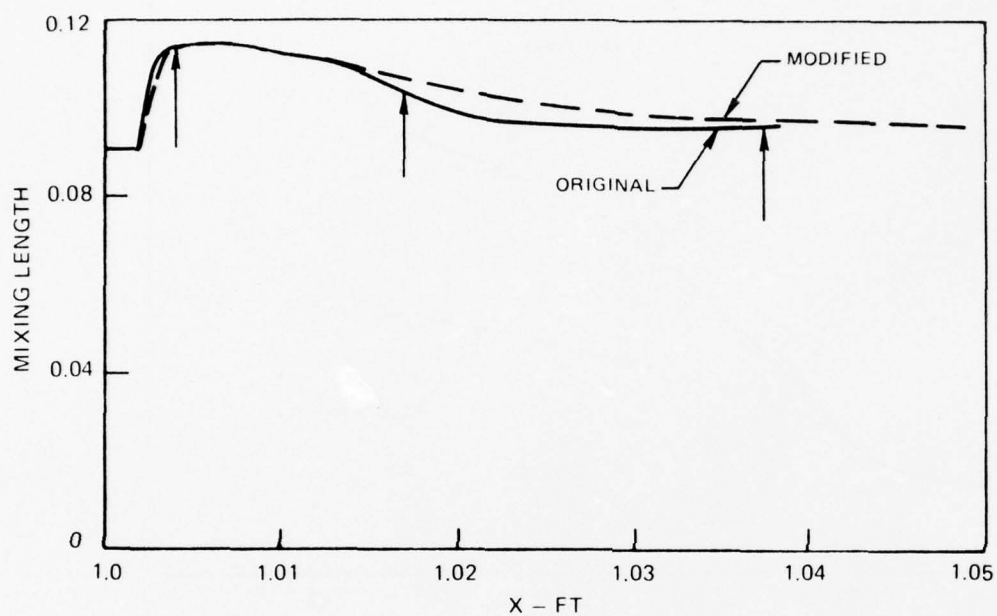


Figure 13. "Equilibrium" Wake Mixing Length Distributions With Low Reynolds Number Correction

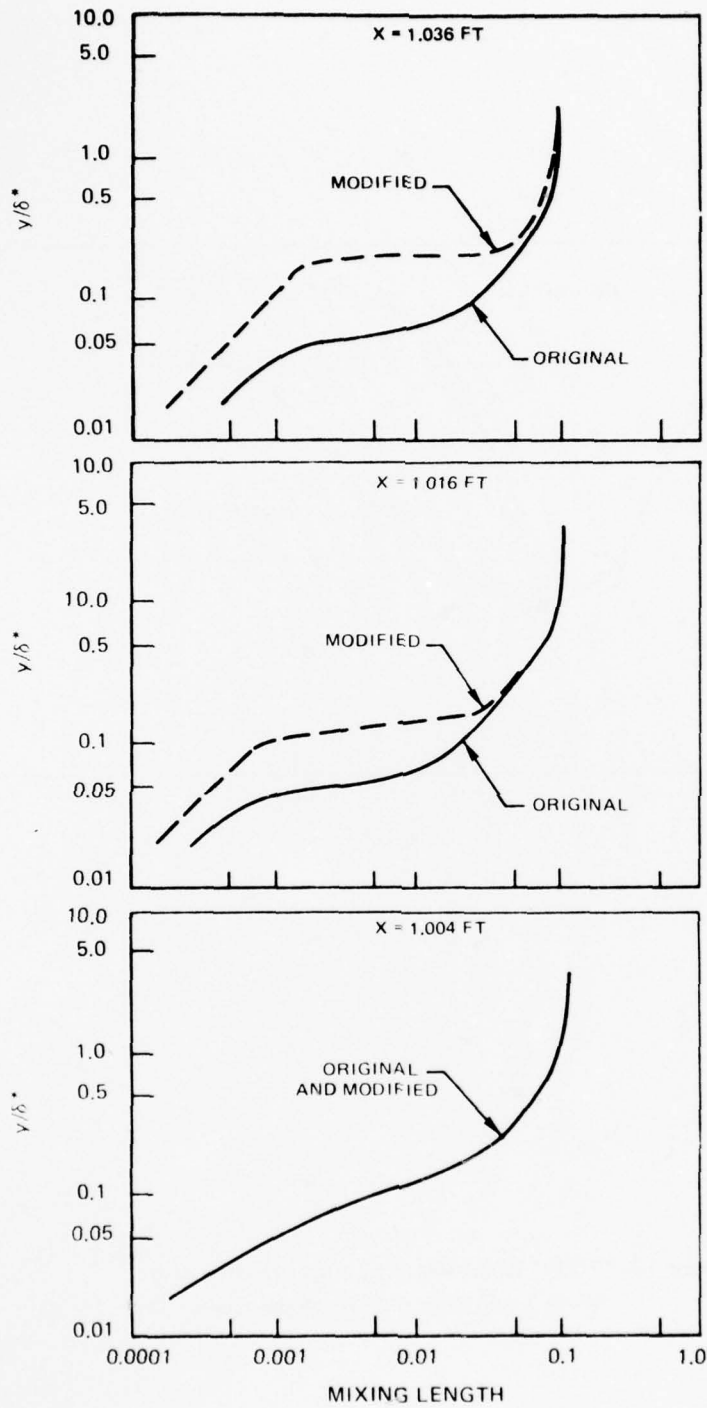


Figure 14. "Equilibrium" Normal Mixing Length Distributions With Low Reynolds Number Corrections

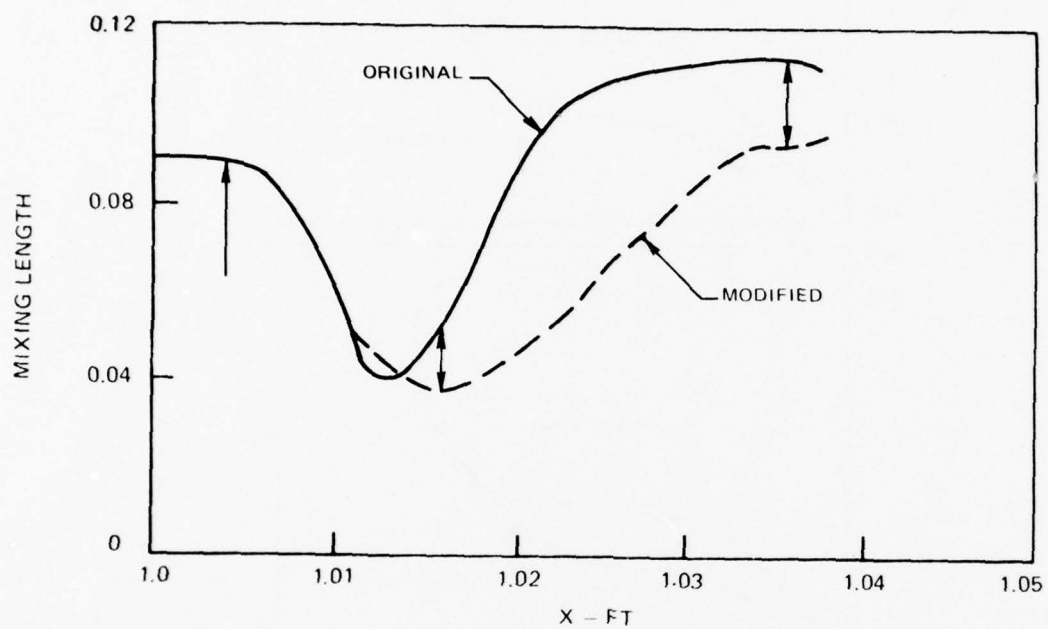


Figure 15. "TKE" Wake Mixing Length Distributions
With Low Reynolds Number Correction

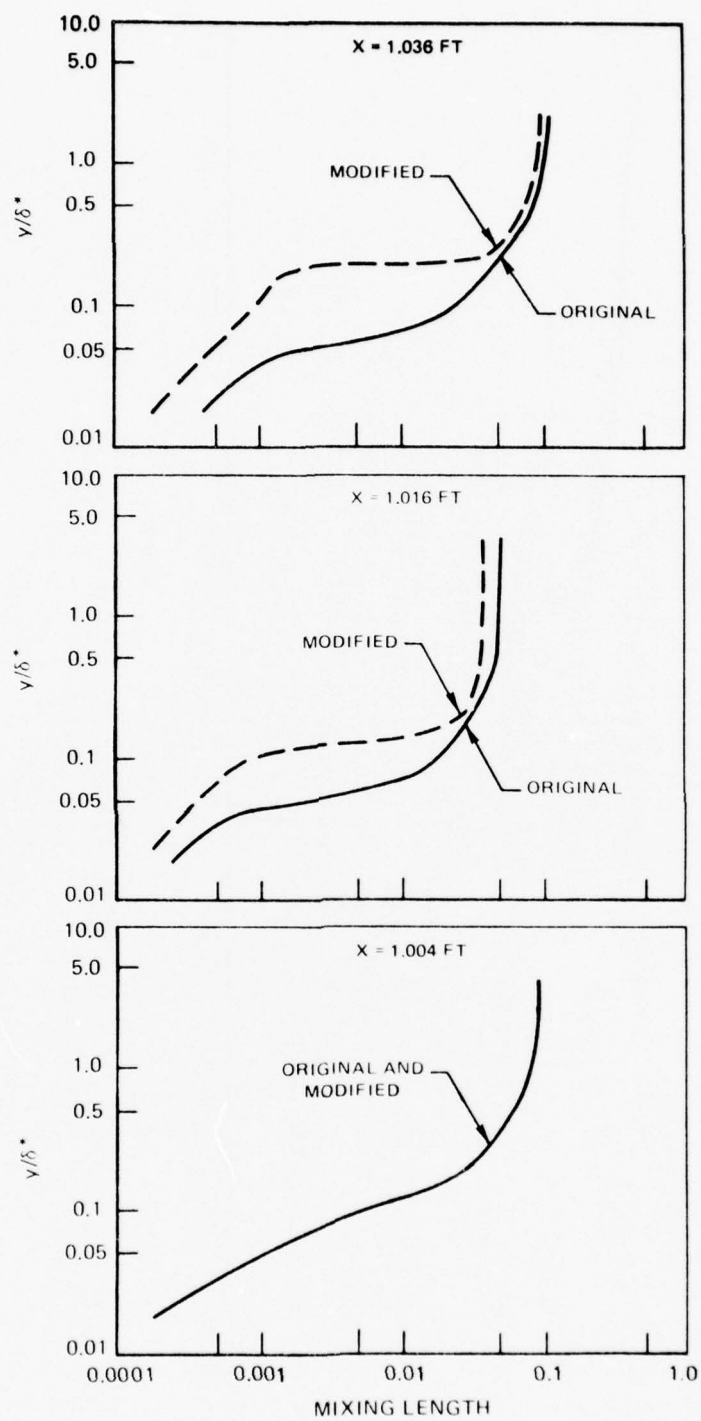


Figure 16. "TKE" Normal Mixing Length Distributions With Low Reynolds Number Corrections

$$M_\infty = 2.93$$

$$Re_{\delta_0} = 3.63 \times 10^4$$

○ DATA OF SPAID AND FRISCHETT (REF. 51)

— MODIFIED TURBULENCE KINETIC ENERGY MODEL

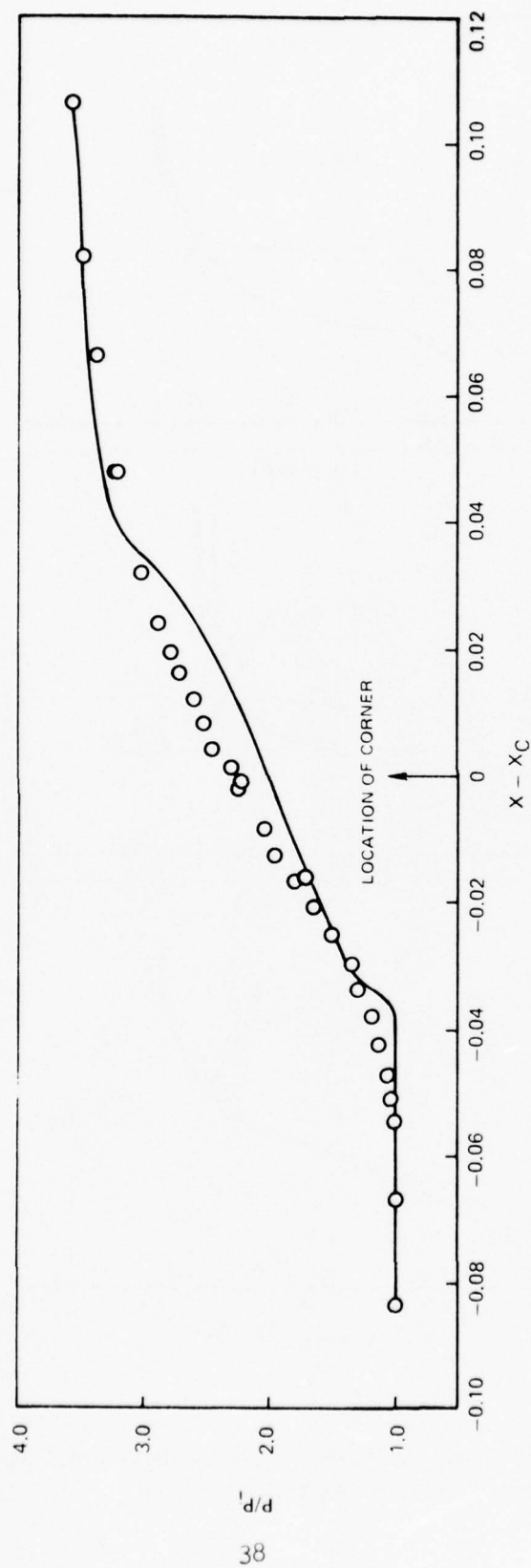


Figure 17. Turbulent Strong Interaction Solution For 19.67° Ramp Using Modified Turbulence Model

$$M_\infty = 2.93$$

$$Re_{\delta_0} = 3.63 \times 10^4$$

○ DATA OF SPAID AND FRISHEIT (REF. 51)

— MODIFIED TURBULENCE KINETIC ENERGY MODEL

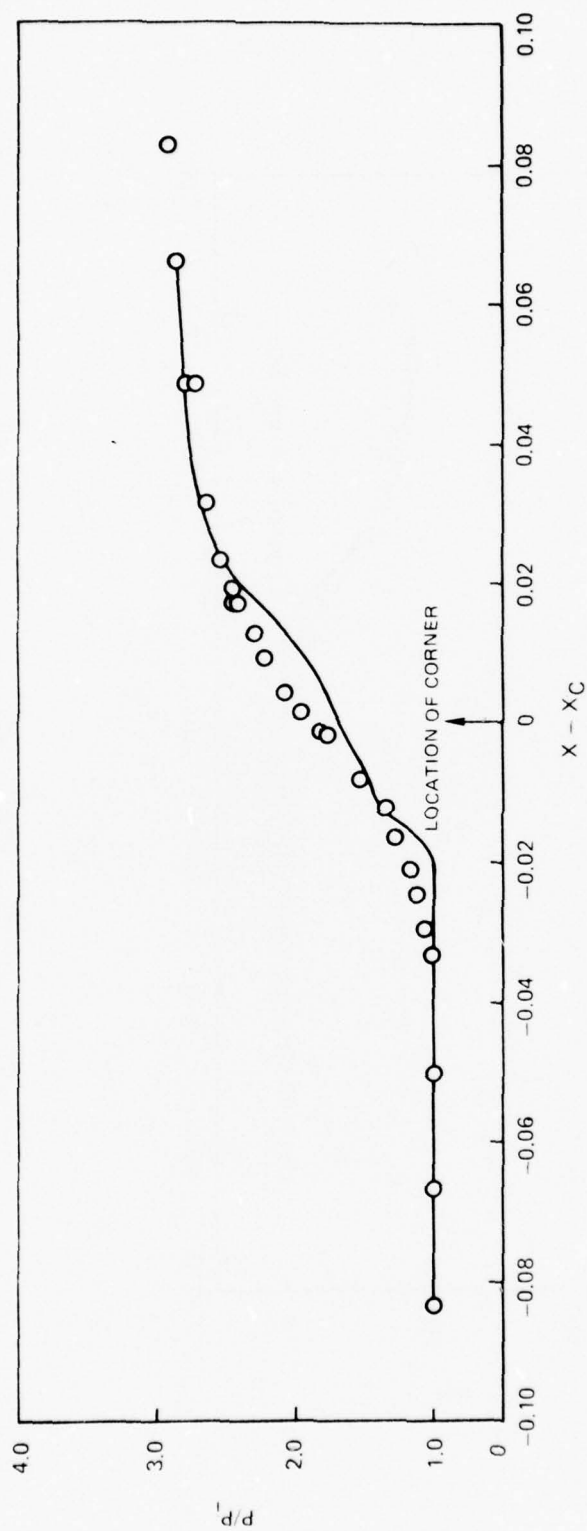


Figure 18. Turbulent Strong Interaction Solution For 16.06° Ramp Using Modified Turbulence Model

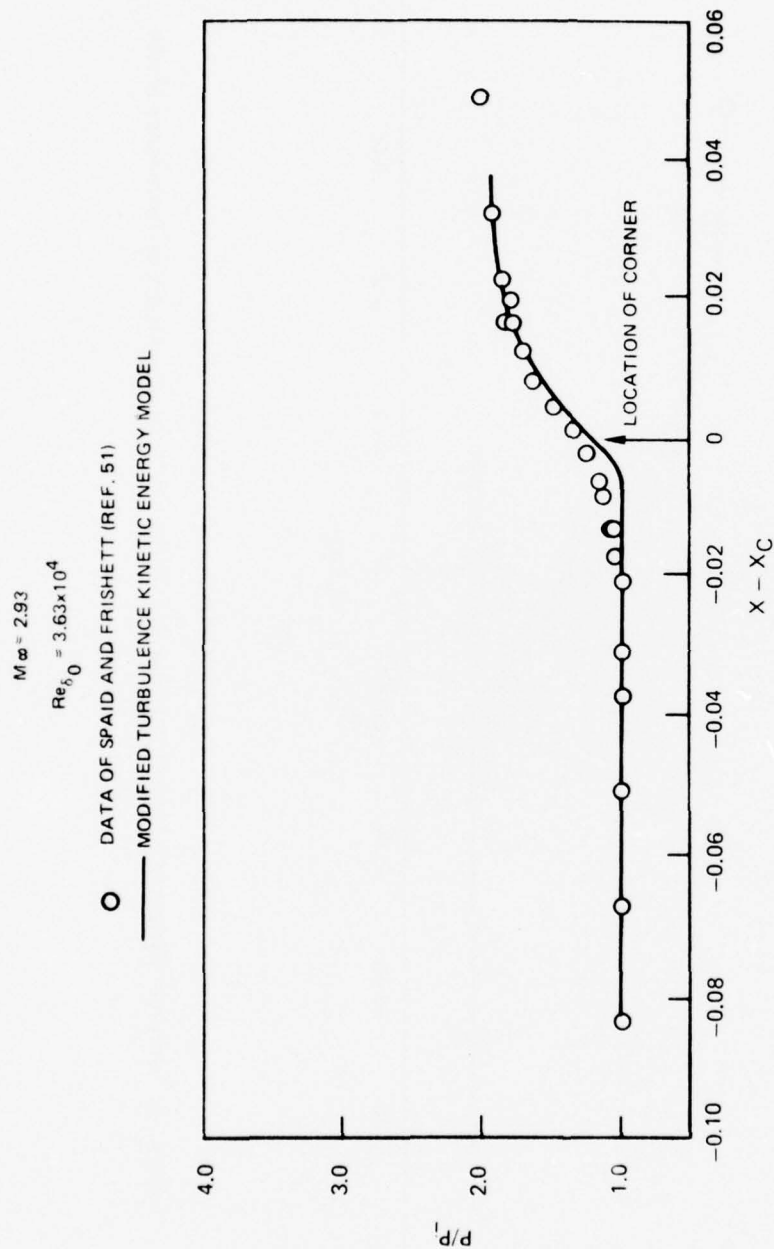


Figure 19. Turbulent Strong Interaction Solution For 9.81° Ramp Using Modified Turbulence Model

THE NAVIER-STOKES APPROACH

The second phase of the present effort is a feasibility study in which the Multi-dimensional Implicit Nonlinear Time-dependent (MINT) procedure of Briley and McDonald (Ref. 9) is applied to the interaction flow field. Until fairly recently it would have been impractical to consider a Navier-Stokes solution to this problem, however, rapid advances both in numerical analysis and computer technology now make the Navier-Stokes procedure a possible alternative to the extended boundary layer procedures for shock wave-boundary layer interaction predictions. Solutions based upon a Navier-Stokes procedure have several advantages over those based upon boundary layer analyses. First of all, solutions based upon the Navier-Stokes equations need not make an arbitrary division between viscous and inviscid portions of the interaction flow field. In addition, Navier-Stokes procedures solve a full transverse momentum equation and need not make any approximation to the convection terms in separated flow regions. These considerations indicate that even if a Navier-Stokes interaction procedure would require more computer resources (storage and run time) than a boundary layer interaction procedure, its potentially increased accuracy may make it an attractive alternative.

In the past few years several investigators have applied Navier-Stokes procedures to the interaction problem (e.g., Refs. 2, 29, 30, 47 and 48). With the exception of MacCormack (Ref. 30), all those solutions have been based upon explicit finite difference procedures. In Ref. 30, MacCormack used a hybrid procedure in which convective terms were treated explicitly and viscous terms treated implicitly. One major difficulty which seems to emerge in varying degrees of severity in Navier-Stokes interaction solutions is the accurate treatment of the shock wave. Over the past years a considerable effort has been expended in developing explicit procedures which can solve the flow equations in the presence of flow discontinuities (shocks). The explicit finite difference interaction procedures mentioned above are based upon such a procedure originally suggested by the weak solution concepts of Lax and developed to a fine point by MacCormack; this procedure is described in detail in Ref. 29. In a separate development Moretti (Ref. 37) treated shock waves as spatial discontinuities with explicit recognition of their presence. However, at the present time this technique cannot be used in viscous regions where the shock can be physically diffracted by the shear layer. To date, no similar large scale shock treatment effort has been undertaken using implicit methods.

In a study of inviscid transonic flow Murman and Cole (Ref. 38) solved the transonic perturbation equations using an implicit line relaxation procedure. The Murman-Cole technique succeeded in capturing shocks in supercritical flow as part of a continuous solution owing largely to the numerical viscosity introduced by the difference scheme. In a later work Murman (Ref. 39) used a special difference operator at the sonic line (the shock point operator) and

again captured the shock as part of a continuous solution. The shock representation in this latter work was considerably sharper than in the Murman and Cole work. Both procedures are discussed in some detail by Hafez and Cheng (Ref. 19). In addition, Beam and Warming (Ref. 4) have used the Briley-McDonald numerical procedure to investigate the flow field about a shock in which the flow passes from a supersonic to a subsonic state. Therefore, although some effort has been expended upon shock representation within implicit schemes, the effort has concentrated primarily upon (i) flows which are inviscid and (ii) shocks through which the flow goes from a supersonic to a subsonic state. Neither of the above requirements is satisfied in the shock wave-boundary layer interaction problem where the flow is viscous and the shock is usually not strong enough to cause subsonic flow on its downstream side. The Navier-Stokes portion of the present effort represents a simple feasibility study in which a fully implicit procedure is applied to the shock wave-boundary layer interaction problem. The study assesses an application of the MINT code, in its present form, to the interaction problem, gives an estimate of computer run times and indicates areas in which further development work would be required to obtain a reliable and accurate prediction procedure.

The Basic Analysis

The Governing Equations

The equations solved in the procedure represent conservation equations of mass, momentum and energy (Ref. 6). For simplicity the equations are expressed in vector notation below and all quantities are nondimensional. Velocities are normalized by U_D , density by ρ_D , enthalpy by h_D , temperature by T_D , pressure by $p_D = \rho_D R_g T_D$ where R_g is the gas constant, dynamic viscosity by μ_D , and time by (L/U_D) where L is the reference length, body forces and bulk viscosity are all assumed to be negligible. The resulting time-averaged equations are given by

Continuity

$$\frac{\partial \rho}{\partial t} = -\nabla \cdot (\rho \vec{u}) \quad (24)$$

Conservation of Momentum

$$\frac{\partial(\rho \vec{u})}{\partial t} = -\nabla \cdot (\rho \vec{u} \vec{u}) - \frac{p_D}{\rho_D U_D^2} \nabla p + \frac{1}{Re} \nabla \cdot (2\mu_{eff} \vec{e}) - \frac{2}{3} \frac{1}{Re} \nabla [\mu_{eff} (\nabla \cdot \vec{u})] \quad (25)$$

Conservation of Energy

$$\begin{aligned} \frac{\partial(\rho H)}{\partial t} = & -\nabla \cdot (\rho \vec{u} H) + \frac{p_D}{\rho_D h_D} \frac{\partial p}{\partial t} + \frac{1}{Re} \nabla \cdot (\Gamma_h \nabla H) \\ & + \frac{1}{Re} \frac{U_D^2}{h_D} \nabla \cdot [(\mu_{eff} - \Gamma_h) \nabla \left(\frac{\vec{u} \cdot \vec{u}}{2} \right)] \end{aligned} \quad (26)$$

The mean flow rate of strain tensor in Eq. (25) is given by

$$\bar{\epsilon} = \frac{1}{2} [(\nabla \bar{u}) + (\nabla \bar{u})^T] \quad (27)$$

The necessary thermodynamic relationships are

$$p = \rho T \quad (28)$$

$$H = h + \frac{1}{2} \frac{u_D^2}{h_D} (\bar{u} \cdot \bar{u}) \quad (29)$$

and for constant specific heat the enthalpy is

$$h = c_p T \quad (30)$$

In order to solve the above system of equations it is necessary to specify the turbulent exchange coefficients μ_{eff} and Γ_h . In the present analysis since the effective Prandtl number is defined from knowledge of turbulent flows of gases, only the turbulent momentum exchange coefficient, μ_{eff} , must be specified. The energy exchange coefficient is obtained from the relation

$$\Gamma_h = \frac{\mu_{eff}}{Pr_{eff}} \quad (31)$$

and the effective viscosity is obtained from a turbulence model.

The Turbulence Model

In the case of laminar flow the governing equations, Eqs. (24) - (26), along with the relations expressed by Eqs. (27) - (31) are sufficient to determine a solution when proper boundary conditions are applied. However, in turbulent flow it is necessary to hypothesize a turbulence model relating the turbulent viscosity to the other problem variables. Over the past years many such models have been hypothesized. These include equilibrium models relating a mixing length or eddy viscosity to local variables, and historical models in which the local turbulent stress is determined through an additional equation (or equations) relating the stress to the upstream history of the flow. A model of the latter type in which a mixing length is hypothesized but in which the magnitude of the mixing length is determined by the turbulence kinetic energy equation is discussed in the boundary layer section of this report.

Since the present Navier-Stokes effort represents an initial feasibility study, a relatively simple turbulence model based upon a mixing length was used. This model is similar to the two-region eddy-viscosity model utilized by Shang and Hankey (Ref. 48), in which the mixing length in the inner region is given by the equilibrium model discussed in Section II, i.e., the turbulent viscosity is

$$\mu_{\tau_i} = \rho \ell^2 \sqrt{2 \underline{\underline{e}} : \underline{\underline{e}}} \quad (32)$$

with the mixing length, ℓ , given by

$$\frac{\ell}{\delta_b} = \frac{\ell_\infty}{\delta_b} \tanh\left(\frac{Ky}{\ell_\infty}\right) \mathcal{D}_s$$

where δ_b is the local boundary layer thickness, K is the von Karman constant, y is the distance from the wall, and \mathcal{D}_s is a sublayer damping factor defined by

$$\mathcal{D}_s = \left[P\left(\frac{y^* - \bar{y}^*}{\sigma^*}\right) \right]^{1/2} \quad (33)$$

where P is the normal probability function, and

$$y^* = y \left(\frac{\tau}{\rho}\right)^{1/2} \frac{\rho}{\mu} \quad (34)$$

Here τ is the local shear stress, $y^+ = 23$ and $\sigma^+ = 8$.

For two-dimensional equilibrium turbulent boundary layers (ℓ_∞/δ_b) has a value of approximately 0.1, which was employed in the calculations reported herein. In addition, because of the difficulty of defining the boundary layer edge in an interacting flow field, δ_b was taken as the boundary layer thickness upstream of the interaction region.

The outer region eddy viscosity is given by the Clauser defect law, i.e.,

$$\mu_{\tau_0} = 0.0168 \rho u_{\max} \delta_{inc}^* \gamma_k \quad (35)$$

where δ_{inc}^* is the kinematic displacement thickness

$$\delta_{inc}^* = \int_0^{\infty} \left(1 - \frac{u}{u_{max}}\right) dy \quad (36)$$

and γ_k is the Klebanoff intermittency which may be approximated by

$$\gamma_k = \left[1 + 5.5 \left(\frac{y}{\delta_b}\right)^6\right]^{-1} \quad (37)$$

In Eqs. (35) - (36), u_{max} has been employed instead of the edge velocity to avoid possible anomalous behavior of the transient solution (Ref. 48).

Artificial Damping

The treatment of shock waves in a Navier-Stokes calculation procedure with finite differences requires the use of artificial diffusion in order to prevent numerical oscillation which may cause solution divergence. In the present implicit procedure a modified form of the fourth-order pressure damping term suggested by MacCormack and Baldwin (Ref. 29) has been employed, viz., a term of the form,

$$D_{p_k} = \eta_k \frac{\partial^2 \phi}{\partial x_k^2} \quad (38)$$

has been added to each of the governing equations being solved for each coordinate direction x_k . The diffusion coefficient η_k in Eq. (38) was taken as

$$\eta_k = \beta (\Delta x_k)^3 f \cdot \frac{|u_k| + c}{4 \bar{p}} \left(\frac{\partial^2 p}{\partial x_k^2} \right) \quad (39)$$

where $0 < \beta \leq \frac{1}{2}$, c is the local sound speed, and the average pressure \bar{p} given by

$$\bar{p} = \frac{1}{4} (p_{i-1} + 2p_i + p_{i+1}) \quad (40)$$

where i is the grid point index in the x_k -direction. In the damping term the factor f is set to 1.6 for the continuity equation and to p for all other conservation equations.

Boundary Conditions

In the present Navier-Stokes calculations boundary conditions were specified along all boundaries of the computational regime. At the wall the normal and tangential velocities were set to zero and a three point one-sided difference form of the continuity equation was applied. At the upstream edge of the calculation region both velocity components as well as the density were specified. These values were determined by performing a calculation over a region extending from a station slightly downstream of the plate leading edge to a station slightly upstream of the location at which the interaction calculation was to be initiated. This calculation yielded a flat plate boundary layer solution that was consistent with the finite difference representation, turbulence model and grid spacing used for the interaction problem. The profiles calculated at the station having the desired boundary layer thickness then were used as upstream boundary conditions for the interaction calculation. At the downstream boundary first derivatives of all dependent variables were set to zero. Finally, both velocity components and the density were set at the outer edge boundary. This boundary was taken at a distance of approximately five boundary layer thicknesses from the wall. An oblique shock was assumed to penetrate the boundary between the third and fourth grid points from the upstream station. The values downstream of the shock were obtained from the oblique shock relations.

The Nonuniform Grid

The accuracy of solutions computed with a given number of grid points often can be improved by using a nonuniform grid spacing to ensure that grid points are closely spaced in regions where the solution varies rapidly. In the interaction flow field large gradients are present near the wall and consequently fine grid resolution is desired in this region. This grid resolution was obtained using an analytic coordinate transformation devised by Roberts (Ref. 42) which is a very effective means of introducing a nonuniform grid when the steep gradients occur near the computational boundaries. Suppose that N grid points are to be used in the range $X_1 \leq X \leq X_2$, and that steep gradients are anticipated in a region of thickness, $\delta (X_2 - X_1)$ near X_1 . Then Roberts' transformation $X_T(X)$ is given by

$$X_T(X) = N + (N-1) \ln \left(\frac{X+b-c}{X+b-c} \right) / \ln \left(\frac{b+a}{b-a} \right) \quad (41)$$

where $a = X_2 - X_1$, $b^2 = a^2/(1 - \beta)$, and $c = X_2$. The use of equally-spaced points in the transformed coordinate, X_T , ensures an adequate resolution of both the overall region $X_1 \leq X \leq X_2$ and the subregion $X_1 \leq X \leq \beta(X_2 - X_1)$. Derivatives with respect to the physical coordinate, X , are obtained from the following formulas:

$$\frac{\partial}{\partial X} = \frac{dX_T}{dX} \frac{\partial}{\partial X_T} \quad (42)$$

$$\frac{\partial^2}{\partial X^2} = \left(\frac{dX_T}{dX}\right)^2 \frac{\partial^2}{\partial X_T^2} + \frac{d^2 X_T}{dX^2} \frac{\partial}{\partial X_T} \quad (43)$$

The use of three-point difference operators for X_T derivatives in Eqs. (33) and (34) produces similar operators for X derivatives. These X -derivative operators can be computed at the start of a calculation and stored, along with the X locations of grid points.

In the present effort rather than use the Roberts transformation over the entire flow regime, the transformation was used only in the vicinity of the wall. In regions away from the wall an equally spaced grid was used. The two regions were matched by requiring that at the join point the physical step size in the transformed regime be the same as the step size in the equally spaced regime. Thus continuity of the spacing was preserved. It should be noted that although the mesh was continuous, its derivative was not and an improved mesh would join the Roberts region to the equally spaced region via a transition region. However, the mesh did not seem to be the cause of any numerical problems and, therefore, the two region mesh was deemed adequate for the present investigation.

Method of Solution

Exact analytical solutions of the Navier-Stokes equations are rare due to their high order and coupled nonlinearity. As a result numerical methods must generally be employed for the solution of these equations. In addition, one of the major obstacles to the solution of the three-dimensional compressible Navier-Stokes equations is the large amount of computer time required, and consequently efficient computational methods are highly desirable. Most numerical procedures used to solve the Navier-Stokes equations have been based on explicit difference schemes for the unsteady form of the governing equations, and are subject to one or more stability restrictions on the size of the time step relative to the spatial mesh size (e.g., Refs. 1, 29 and 43). These stability limits usually correspond to the well-known Courant-Friedrichs-Lewy (CFL) condition and in some methods to an additional viscous stability condition. A

key disadvantage of such conditionally stable methods is that the maximum time step is fixed by the spatial mesh size rather than the physical time dependence. If a steady solution is being computed as the asymptotic limit of the unsteady solution, then using a small time step requires a large number of steps to reach the steady solution.

In contrast to most explicit methods, many implicit methods tend to be stable for large time steps, and hence, offer the prospect of substantial increases in computational efficiency, provided of course that the computational effort per time step is competitive with that of the conditionally stable methods. An accurate and efficient implicit method termed the MINT procedure has been developed at UTRC by Briley and McDonald (Ref. 9) for solution of the three-dimensional, compressible Navier-Stokes equations. This procedure since has been used for further studies of rectangular duct flow by Briley, McDonald and Gibeling (Ref. 10) and for three-dimensional combustor flow calculations by Gibeling, McDonald and Briley (Ref. 18). The Navier-Stokes portion of the present study is based upon a two-dimensional version of the MINT code. In brief, this procedure first linearizes the equations by expanding the solution at a known time level, n , to represent the solution at time level $n+1$. The resulting linear equations are solved using an alternating direction implicit (ADI) method. A description of this numerical procedure is presented in Appendix D. More detailed descriptions are presented in Refs. 9, 10 and 18.

Results of Navier-Stokes Computations

Several sample cases were considered in assessing the ability of the MINT code to make predictions of the shock wave-boundary layer interaction flow field. The shock impingement problem was considered herein since some experimental data are available (Law, Ref. 26), and this problem has been considered previously by other investigators (e.g., Refs. 29 and 48). The flow conditions upstream of the incident shock wave were chosen to correspond as closely as possible to Law's experiment (Ref. 26). Incident shock waves of strength $p_2/p_1 = 2$ (case 1, $\theta_s = 27.4^\circ$) and $p_2/p_1 = 3$ (case 2, $\theta_s = 33.8^\circ$) were considered, where p_1 is the static pressure upstream of the shock, p_2 is the static pressure downstream of the shock, and θ_s is the shock angle. The former case corresponds approximately to the shock generator angle of 9.87° examined by Refs. 26 and 48.

The flow field in the present analysis is divided into two overlapping computational domains following the procedure used in Ref. 48. In the first domain the turbulent boundary layer development over a flat plate was calculated. A 36×40 computational grid covering a physical domain of approximately 58×608 was employed in the boundary layer calculation. The interaction region is contained in the second computational domain. For case 1 a 36×61 computational grid was employed for a domain of about 58×208 , and for case 2 a 36×56 grid was employed for a domain of about 58×178 . A Roberts grid transformation was used in the normal coordinate direction with 23 points in the inner region ($\Delta y_{\min} = 0.0063$ mm), and 13 points in the constant mesh-spacing outer region ($\Delta y = 1.09$ mm). The streamwise grid spacing in the boundary layer calculation (first computational domain) was $\Delta x = 5.6$ mm, while in the interaction domain the spacing was $\Delta x = 1.22$ mm for case 1 and $\Delta x = 1.14$ mm for case 2.

In this feasibility study, computation times on a CDC 6600 were approximately one hour per case to reach convergence. However, the cases were run with a generalized code capable of performing calculations both in three dimensions and with orthogonal curvilinear coordinates and no serious effort was made to optimize either the code or the time step for this particular problem. If the code were rewritten to apply specifically to a Cartesian system, it is estimated that the run times would be reduced by approximately a factor of two. In regard to optimization of the time step, in the limited amount of time and effort available a detailed study concentrating on time step optimization for this type of problem was not possible and a rather conservative time step selected which doubtless did not take full advantage of the large time step capabilities inherent in the present implicit procedure. Finally, solution oscillations related both to the shock representation and the turbulence model (which are discussed subsequently) may also have increased the case running time. Based upon these initial runs, it is estimated that a streamlined Cartesian deck with an optimum time step could perform an interaction calculation in 15 to 25 minutes of CDC 6600 run time with about 2200 mesh points. Finally, it should be noted that the present calculations were run with a grid definition in the near wall region much better than that usually used in stability restricted explicit calculations. For example, the grid spacing in the immediate vicinity of the wall used in the present effort was approximately one-fifth of that used by Shang, Hankey, and Law (Ref. 48). This improvement in grid definition obtained in the present effort without an accompanying penalty in computer run time was made possible by the favorable stability properties of implicit methods. In the upstream boundary layer, the grid employed in the present effort contained two points in the region $y^+ < 7$. Based upon our experience with classical boundary layer solutions, one point is required in the region $y^+ < 7$ to obtain skin friction predictions which are accurate to within 10 percent.

The sample cases pointed out several deficiencies in the "shock capturing" treatment of shock waves. As noted by Shang, Hankey, and Law (Ref. 44) there is significant smearing of the incident shock wave in the relatively coarse mesh which must be employed in a Navier-Stokes calculation. This shock resolution problem appears to be more pronounced in the current implicit procedure than it was in explicit procedures based upon MacCormack's method. However, this is not surprising since MacCormack's method was developed for shock calculations over a period of many years, whereas the present work is the first application of the MINT procedure to flow fields containing shock waves. The present results should not be construed as indicating an inherent limitation of implicit schemes to resolve shock waves, they imply that at this stage of development they do not capture shocks quite as well as some of the explicit schemes. Obviously, much further work aimed at applying implicit techniques to shock wave problems needs to be done.

Plots of skin friction coefficient and surface pressure are shown in Figs. 20a and 20b for case 1 ($p_2/p_1 = 2$) and in Figs. 21a and 21b for case 2 ($p_2/p_1 = 3$). Although both experimental data as well as the explicit calculations of Shang, Hankey, and Law (Ref. 48) indicate separation under these conditions, the present calculations do not. There are several possible reasons for this discrepancy. First, as previously stated, the shock smearing problem in the present implicit calculation appears to be more severe than in explicit calculations performed to date. Secondly, a more sophisticated turbulence model than that which was used may be required. Finally, in comparison with the calculations of Ref. 48, the present procedure had a much better definition of the flow in the wall region. It is not clear what the effect of improving the grid definition in the explicit method would have upon the explicit calculation results and, therefore, a direct comparison between the present implicit calculation and the explicit calculation of Ref. 48 is somewhat difficult. The experimental surface pressure distribution for case 1 is also shown in Fig. 20b, from which it is apparent that the initial rapid rise of surface pressure which accompanies separation is not predicted very well by the present calculations. This seems to be directly related to the smearing of the incident shock wave and is believed to be closely connected with the lack of separation in this case.

Since the pressure ratio $p_2/p_1 = 2$ case did not separate, a stronger shock calculation having a pressure ratio of 3 was considered. As shown in Fig. 21b, the shape of the predicted pressure rise showed the rapid initial increase expected in interaction flow fields. Furthermore, the level of the downstream wall pressure was essentially the inviscid value. The predicted length of the separated region was shorter than expected, a result consistent with the lack of separation observed in the pressure ratio $p_2/p_1 = 2$

calculation. Finally, the skin friction distribution in the separated case (Fig. 21a, $p_2/p_1 = 3$) is also qualitatively reasonable, although the increase in skin friction downstream of the incident shock was unexpected. This may be due to the turbulence model incorporated in the present procedure.

Several problems have been encountered in the present study which require further investigation. First of all, shock resolution in the implicit framework must be improved, since the resolution obtained with the present formulation is apparently not as good as that obtained using MacCormack's alternating-direction-explicit method (e.g., Refs. 29 and 48). Also, some oscillation of the solution about the steady-state has been observed, especially in the sublayer. This problem may be partially related to both the turbulence model and the choice of time step. Further investigation into the optimal choice of the time step for this implicit procedure should be carried out, since it is believed that a significant improvement in the convergence rate can be realized. Finally, the present calculations were obtained using primitive variables (ρ, u, v, h) rather than conserved variables ($\rho, \rho u, \rho v, \rho(e + \frac{1}{2}q^2)$) which may have resulted in additional smearing of the incident shock wave. Hence, in future studies consideration should be given to using conserved variables.

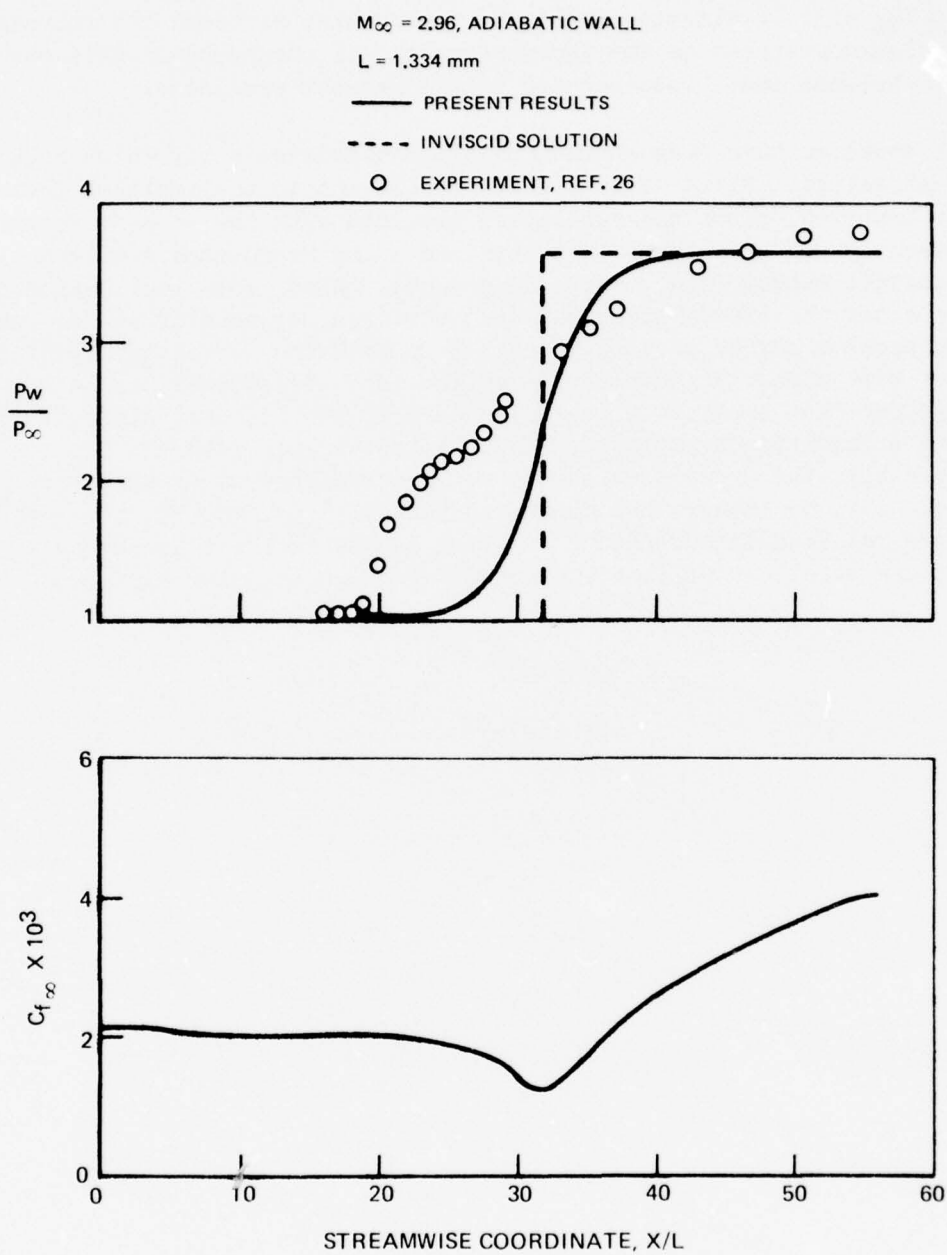


Figure 20. Navier - Stokes Interaction Calculation, $P_2/P_1 = 2$

77-02-51-2

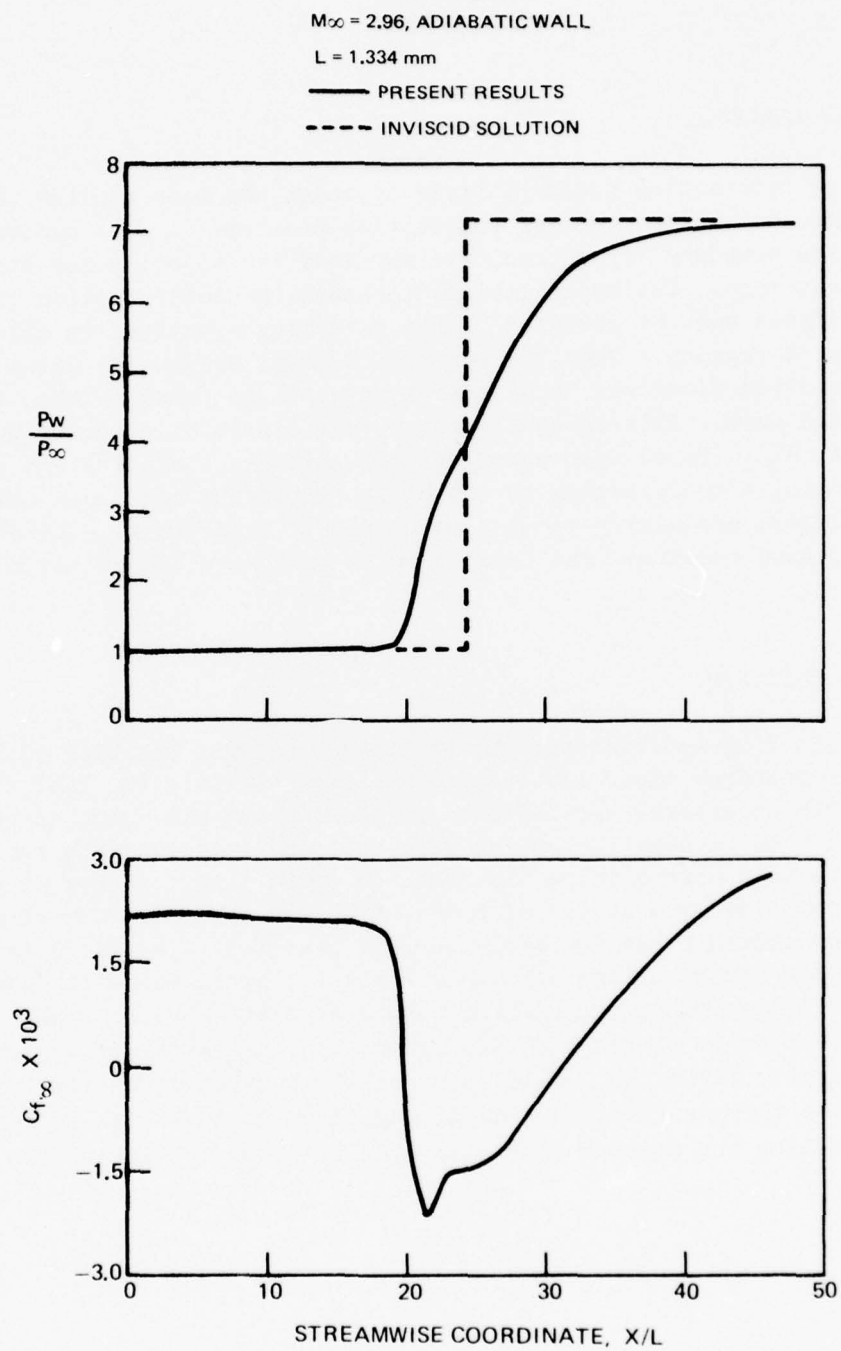


Figure 21. Navier - Stokes Interaction Calculation, $P_2/P_1 = 3$

SECTION III CONCLUSIONS

BOUNDARY LAYER ANALYSIS

The strong interaction boundary layer approach has been applied to the shock wave turbulent boundary layer interaction problem. A well proven weak interaction boundary layer procedure was modified to allow for strong interaction solutions. The modifications included the incorporation of an outer flow analysis and the revision of the governing equations to allow for flow in separated regions. When the turbulence model originally developed for weak interaction flows was used, poor agreement was found between the calculations and data. This is consistent with the results reported by Shang and Hankey (Ref. 47). Based upon computational turbulence studies and recent experimental data, a modification to the basic turbulence model was developed for boundary layers containing recirculating flow. Using this modified turbulence model, good agreement was found between the calculations and test data.

NAVIER-STOKES ANALYSIS

An implicit finite-difference Navier-Stokes analysis has been applied to the shock wave-boundary layer interaction problem. Despite the fact that the code was written in general curvilinear coordinates and was not streamlined for the interaction problem, solutions were obtained in reasonable run times. Indications are that streamlining the code and optimizing the time step could decrease the run time by a factor of four. Although solutions for strong incident shocks showed a qualitatively correct behavior (i.e., skin friction and wall pressure distributions were in qualitative agreement with data), the procedure severely smoothed the incident shock wave thus suppressing separation for moderate shocks and underpredicting the extent of separation for strong shocks. Therefore, calculation of shock waves in an implicit method requires further investigation. In addition, further work in regard to turbulence modeling and optimum time step specification is warranted.

APPENDIX A

WEAK INTERACTION CALCULATION PROCEDURE

The procedure used to solve the momentum and energy equations is a Hartree-Womersley calculation procedure similar to that described by Smith and Clutter (Ref. 50). In the calculation procedure the differential equations are transformed to a form more convenient for computer solution by introducing new variables

$$\eta = y/\delta^+ \quad (A-1)$$

$$F' = 1 - \frac{\bar{\rho} \bar{u}}{\rho_e u_e} \quad (A-2)$$

$$G' = \frac{T_e^0 - \bar{T}^0}{T_e^0 - T_{REF}} \quad (A-3)$$

$$\beta = \rho_e / \rho \quad (A-4)$$

where the primes indicate differentiation with respect to η , T^0 is the stagnation temperature, T_{REF} is a specified constant reference temperature, and δ^+ is a length scale usually taken to be the displacement thickness. In certain flows, such as the boundary layer developing on the cold wall nozzle, the displacement thickness may become small or even negative and in these cases δ^+ is taken to be a linear combination of the displacement thickness and a constant reference length such that δ^+ remains positive.

The momentum equation, Eq. (9), and the energy equation, Eq. (10), are solved by first eliminating $\bar{\rho} \bar{v}$ through the continuity equation, Eq. (3), and replacing the variables T^0 , ρ , and u by G' , F , and β . The streamwise derivatives are then replaced by finite differences leading to equations of the form

$$A_3 F''' + A_2 F'' + A_1 F' + A_0 F = A_4 \quad (A-5)$$

$$B_3 G''' + B_2 G'' + B_1 G' = B_4 \quad (A-6)$$

where A_n and B_n are functions of F , G' and their derivatives. The equations are linearized by assuming values for F , G' and their derivatives based upon the solution at the previous streamwise stations and the resulting linear differential equations are solved by Gaussian elimination using the boundary conditions

$$F'(0) = 1 - \frac{\rho_w u_w}{\rho_e u_e} \quad (A-7)$$

$$F'(\delta) = 0 \quad (A-8)$$

$$G'(0) = \frac{T_{\theta}^0 - T_w}{T_{\theta}^0 - T_{REF}} \quad \text{OR} \cdot G''(0) = 0 \quad (A-9)$$

$$G'(\delta_{TH}) = 0 \quad (A-10)$$

where δ_{TH} is the thickness of the thermal boundary layer. In the calculations presented in the present report, u_w was always taken as zero. Having obtained the solution of the linearized equations, the distributions of F and G' are compared to the distributions used to evaluate the nonlinear coefficients, A_n and B_n . If the old and new distributions agree to within a specified tolerance, the procedure moves to the next streamwise station. If the two do not agree, the procedure is repeated. In the case of turbulent flow, the coefficients A_n and B_n , also depend on the turbulent kinematic viscosity, ν_T , and a turbulence kinetic energy equation is included in the iteration loop.

APPENDIX B

BOUNDARY LAYER MODIFICATIONS FOR δ^* SPECIFIED

To specify the displacement thickness, δ^* , and evaluate the static pressure from the momentum equation, a relation containing δ^* was derived to replace the pressure gradient terms in the momentum equation. A parameter, Q , was introduced to represent the naturally occurring term:

$$Q = \frac{\delta^*}{\rho_e} \frac{\partial}{\partial x} (\rho_e u_e \delta^*) \quad (B-1)$$

Q was then treated as one of the dependent variables and terms containing products of Q and other dependent variables were linearized in the usual manner.

From isentropic relations it can be shown that

$$\frac{1}{\rho_e} \frac{\partial \rho_e}{\partial x} = \frac{u_e}{(\gamma - 1) C_p T_e} \frac{\partial u_e}{\partial x} \quad (B-2)$$

Expanding the definition of Q yields

$$Q = u_e \delta^* \frac{\partial \delta^*}{\partial x} + \delta^{*2} \left(1 - \frac{u_e^2}{(\gamma - 1) C_p T_e} \right) \frac{\partial u_e}{\partial x} \quad (B-3)$$

Solving for $\frac{\partial u_e}{\partial x}$

$$\frac{\partial u_e}{\partial x} = (Q - u_e \delta^* \frac{\partial \delta^*}{\partial x}) / \left[\delta^{*2} \left(1 - \frac{u_e^2}{(\gamma - 1) C_p T_e} \right) \right] \quad (B-4)$$

which is of the linear form:

$$\frac{\partial u_e}{\partial x} = T_1 Q + T_2 \quad (B-5)$$

When specifying the displacement thickness, δ^* , T_1 and T_2 in Eq. (B-5) are evaluated and the linear relation in Q is used to replace $\partial u_e / \partial x$ in the pressure gradient terms of the momentum equation.

The momentum equation is solved for the δ^* specified case by linearizing the partial differential equations and replacing derivatives by differences at each grid point. The resulting set of algebraic equations is then solved for the value of the stream function, F , at each grid point and for the parameter Q . The solution is obtained by a modified Gaussian elimination which solves a quin-diagonal matrix with an additional column.

APPENDIX C

ORIGINAL TURBULENCE MODEL USING THE TURBULENCE KINETIC ENERGY EQUATION

As shown in Ref. 46, the boundary layer approximation to the turbulence kinetic energy equation is given by

$$\begin{aligned} \frac{\partial}{\partial x} \left(\frac{1}{2} \bar{\rho} \bar{u} \bar{q}^2 \right) + \frac{\partial}{\partial y} \left(\frac{1}{2} \bar{\rho} \bar{v} \bar{q}^2 \right) &= \underbrace{-\bar{\rho} \overline{u'v'}}_{\text{advection}} \frac{\partial \bar{u}}{\partial y} \quad \underbrace{-\bar{\rho} \epsilon}_{\text{production}} \\ &\quad \underbrace{-\frac{\partial}{\partial y} (\bar{\rho}'v') + \frac{1}{2} (\bar{\rho}v')' \bar{q}^2)}_{\text{diffusion}} - \bar{\rho} \epsilon \\ &\quad \underbrace{-\bar{\rho} (\bar{u}'^2 - \bar{v}'^2) \frac{\partial \bar{u}}{\partial x}}_{\text{normal stress production}} + \underbrace{\bar{\rho}' \frac{\partial u'_i}{\partial x_i}}_{\text{pressure-dilatation}} \end{aligned} \quad (C-1)$$

All calculations reported in the investigation were made with the usual assumption of zero pressure-dilatation contribution to the energy balance (Ref. 8) unless otherwise stated. The turbulence model is developed by integrating Eq. (C-1) with respect to y between the limits $y = 0$ and $y = \delta$ which leads to

$$\begin{aligned} \frac{1}{2} \frac{d}{dx} \int_0^\delta \bar{\rho} \bar{u} \bar{q}^2 dy &= \int_0^\delta -\bar{\rho} \overline{u'v'} \frac{\partial \bar{u}}{\partial y} dy - \int_0^\delta \bar{\rho} \epsilon dy \\ &\quad - \int_0^\delta \bar{\rho} (\bar{u}'^2 - \bar{v}'^2) \frac{\partial \bar{u}}{\partial x} dy + \int_0^\delta \bar{\rho}' \frac{\partial u'_i}{\partial x_i} dy + E \end{aligned} \quad (C-2)$$

where

$$E = \left[\frac{1}{2} \bar{q}^2 \left(\bar{\rho} \bar{u} \frac{\partial \delta}{\partial x} - \bar{\rho} \bar{v} \right) - \bar{\rho}' \bar{v}' \frac{1}{2} (\bar{\rho} v')' \bar{q}^2 \right]_e \quad (C-3)$$

Following Townsend (Ref. 48) and Bradshaw and Ferris (Ref. 8) structural coefficients a_n and L are introduced, together with a mixing length ℓ ; these scales are defined as

$$\begin{aligned} -\overline{u'v'} &= a_1 \bar{q}^2, \quad \overline{u'^2} = a_2 \bar{q}^2, \quad \overline{v'^2} = a_3 \bar{q}^2, \\ \overline{w'^2} &= (1 - a_2 - a_3) \bar{q}^2 \\ \epsilon &= (-\overline{u'v'})^{3/2} / L, \quad (\overline{u'v'})^{1/2} = \ell \frac{\partial \bar{u}}{\partial y} \end{aligned} \quad (C-4)$$

For fully-developed turbulence the structural coefficients a_1 , a_2 , and a_3 are assumed constant having values 0.15, 0.50, and 0.20, respectively (Refs. 7 and 31). Using Eq. (C-4), Eq. (C-3) is put in the form

$$\frac{d}{dx} \left(\frac{\phi_1 \rho_\theta u_\theta^3 \delta^+}{2 a_1} \right) = \rho_\theta u_\theta^3 \left(\phi_2 - \phi_3 + \frac{E}{\rho_\theta u_\theta^3} \right) + \int_0^\delta \bar{\rho}' \frac{\partial u'_i}{\partial x_i} dy \quad (C-5)$$

where

$$\phi_1 = \int_0^{\delta/\delta^*} \frac{\bar{\rho} \bar{u}}{\rho_e u_e} \left(\frac{1}{\delta^*} \frac{\partial \bar{u}/u_e}{\partial \eta} \right)^2 d\eta \quad (C-6)$$

$$\phi_2 = \int_0^{\delta/\delta^*} \frac{\bar{\rho}}{\rho_e} \left(\frac{1}{\delta^*} \right)^2 \left(\frac{\partial \bar{u}/u_e}{\partial \eta} \right)^3 \left(1 - \frac{1}{L} \right) d\eta \quad (C-7)$$

$$\phi_3 = \int_0^{\delta/\delta^*} \frac{\bar{\rho}}{\rho_e} \left(\frac{a_2 - a_3}{a_1} \right) \left(\frac{1}{\delta^*} \frac{\partial \bar{u}/u_e}{\partial \eta} \right)^2 \frac{\delta}{u_e} \frac{\partial \bar{u}}{\partial x} d\eta \quad (C-8)$$

where η is a nondimensional transverse distance y/δ^* , δ^* is an arbitrary reference length, and δ the boundary layer thickness.

The left-hand side of Eq. (C-5) represents the streamwise rate of change of turbulence kinetic energy and is derived directly from the turbulence kinetic energy advection term. The term $\rho_e u_e^3 \phi_2$ represents the integral of turbulence production minus dissipation and $\rho_e u_e^3 \phi_3$ is the normal stress production. The terms designated by E are turbulent source terms resulting from disturbances imposed upon the boundary layer by the free stream. As shown in Eq. (C-3), E is the sum of two major contributions, the first $(q^2/2)(\bar{\rho} \bar{u} \partial \delta / \partial x - \bar{\rho} \bar{v})$ representing the free-stream velocity disturbance (i.e., free-stream turbulence entrained by the boundary layer) and the second, $P'v' + (\bar{\rho} \bar{v})' q^2/2$, representing the direct absorption of acoustic energy.

For fully-developed turbulent flow, as in Ref. 31, L and ℓ are given by

$$\frac{L}{\delta} = 0.1 \tanh [\kappa y / (0.1 \delta)] \quad (C-9)$$

$$\frac{\ell}{\delta} = \frac{\ell_\infty}{\delta} \tanh [\kappa y / \ell_\infty] \quad (C-10)$$

where ℓ_∞ is the "wake" value of the mixing length at any particular streamwise station. Although Eqs. (C-9) and (C-10) give accurate representations of ℓ and L through most of the turbulent boundary layer, it is well-known that they overestimate the length scales within the viscous sublayer and are somewhat inaccurate at low Reynolds numbers. Following McDonald and Fish (Ref. 33) the experimentally observed damping effect in the viscous sublayer is modeled by assuming intermittent turbulence within the sublayer leading to the relation

$$-\overline{u'v'} = \Gamma (-\overline{u'v'})_\tau = \Gamma (\ell \partial \bar{u} / \partial y)_\tau = \left(\mathcal{D} \ell_\tau \frac{\partial \bar{u}}{\partial y} \right)^2 \quad (C-11)$$

In. Eq. (C-6) Γ is the intermittency factor, \mathcal{D} the damping factor, and the subscript T indicates the value with turbulent flow. Obviously, \mathcal{D} is equal to the square root of Γ . As in Ref. 33, the present investigation assumes that the damping distributes normally about a mean height $y^+(y^+ = y\sqrt{T/\rho/\nu})$ with a standard deviation σ leading to the equation

$$\mathcal{D} = P^{1/2} \{ (y^+ - \bar{y}^+) / \sigma \} \quad (C-12)$$

where P is the normal probability function; \bar{y}^+ is taken as 23, and σ as 8. A detailed discussion of the sublayer damping treatment is presented in Ref. 33. In the present calculations the von Karman constant κ was taken to be 0.43.

In regard to the low Reynolds number effects, Coles (Ref. 12) has observed and correlated the departure of the mean velocity profile of a flat plate turbulent boundary layer from the usual similarity laws known to hold at higher Reynolds numbers. Using Coles' correlation of the mean velocity profile in the low Reynolds number regime, McDonald (Ref. 31) integrated the boundary layer equations of mean motion to obtain local distributions of turbulent shear stress and evaluated the local mixing length distributions from the assumed mean velocity distribution and the computed shear stress distributions. Based upon these calculations, a low Reynolds number correction for the dissipation length of the form

$$L = L_\infty [1 + \exp(-1.63 \ln R_\theta + 9.7)] \quad (C-13)$$

was derived where L_∞/δ is given by Eq. (C-9). In the calculations presented in the present report the dissipation length used was obtained by multiplying Eq. (C-13) by the sublayer damping factor, \mathcal{D} .

When numerical values of the structural coefficients a_n are specified, Eqs. (C-10), (C-12), and (C-13) are used to represent L and l , and the pressure dilatation is either neglected or modeled, the turbulence kinetic energy equation, Eq. (C-2), becomes an ordinary differential equation with the dependent parameter $\epsilon_\omega(x)$ which is solved in conjunction with the boundary layer momentum and energy equations to predict the development of both the mean flow field and the turbulent shear stress.

In addition to including the turbulence kinetic energy equation in the set of equations governing the boundary layer development it is necessary to specify a model for turbulent heat flux contribution, $\overline{\rho C_p v' T'}$. As previously stated, in the present procedure, $\overline{v' T'}$ is specified by assuming a turbulent Prandtl number, Pr_T , which relates the velocity-temperature correlation, $\overline{v' T'}$, to the Reynolds stress, $\overline{u' v'}$, through Eq. (8). The turbulent

Prandtl number distribution used in the present procedure varies with distance from the wall in the manner suggested by Meier and Rotta (Ref. 35). As this juncture it should be pointed out that an alternative procedure can be used to determine $\overline{v'T'}$, based upon an easily derived conservation equation for either the quantity $\overline{T'^2}$ or the correlation, $\overline{v'T'}$, which is similar in form to the turbulence kinetic energy equation, Eq. (23). However, to solve this new conservation equation it is necessary to assume a universal structure relating quantities analogous to dissipation, production, etc. While sufficient experimental data exists to allow valid modeling of the required terms for the turbulence kinetic energy equation, the existing data does not indicate how proper modeling could be carried out for the $\overline{v'T'}$ conservation equation. Thus, at least for the present, the approach based upon a turbulent Prandtl number appears preferable to an approach based upon the $\overline{v'T'}$ conservation equation.

APPENDIX D

THE MINT CALCULATION PROCEDURE

The MINT calculation procedure represents an efficient solution to the multi-dimensional, time-dependent Navier-Stokes equations. The procedure is presented in detail in Refs. 9, 10 and 18; for convenience it is presented in condensed form in this appendix. As a prelude to this discussion it is convenient to define a difference notation. For the present it is assumed that the flow region is three-dimensional and is discretized by grid points having equal spacings Δx_1 , Δx_2 and Δx_3 in the x_1 , x_2 and x_3 directions respectively; in addition the time step is Δt . Reduction to two dimensions will be obvious as the discussion proceeds and provisions for nonuniform grids will be introduced at the end of this appendix.

The subscripts i, j, k and superscript n are grid point indices associated with x_1 , x_2 , and x_3 , and t , respectively. Thus $\phi_{i,j,k}^n$ denotes $\phi(x_{1i}, x_{2j}, x_{3k}, t^n)$ where ϕ can represent any of the dependent variables. The subscripts are frequently omitted if clarity is preserved, so that ϕ^n is equivalent to $\phi_{i,j,k}^n$. For convenience, the following shorthand difference-operator notation is used for derivative difference formulas:

$$\delta_1 \phi^n = \frac{-\phi_{i-1,j,k}^n + \phi_{i+1,j,k}^n}{2 \Delta x_1} = \left. \frac{\partial \phi}{\partial x_1} \right|_{i,j,k}^n + O(\Delta x_1)^2 \quad (D-1)$$

$$\delta_1^2 \phi^n = \frac{\phi_{i-1,j,k}^n - 2\phi_{i,j,k}^n + \phi_{i+1,j,k}^n}{(\Delta x_1)^2} = \left. \frac{\partial^2 \phi}{\partial x_1^2} \right|_{i,j,k}^n + O(\Delta x_1)^2 \quad (D-2)$$

with analogous definitions for δ_2 , δ_2^2 , δ_3 and δ_3^2 . It is assumed that the solution is known at the n level, t^n , and is desired at the $(n+1)$ level, t^{n+1} .

LINEARIZATION

The large time-step capabilities of implicit methods can place great demands on the linearization technique employed. Indeed, the favorable stability properties of implicit methods can be severely compromised by an inadequate linearization. The technique used in the MINT code permits the implicit solution of coupled nonlinear equations in one space dimension by a one-step noniterative procedure. This feature is retained for multidimensional problems by using ADI techniques. The linearization is accurate when variables change by relatively small amounts during a time step, and consequently, the accuracy of the linearization can be controlled by varying the time step. The linearization technique is also convenient for the implicit treatment of coupled nonlinear boundary conditions, and this latter feature has been found to have a highly favorable effect on the stability of the overall method (Ref. 9).

For demonstration purposes the technique now will be described for the following first order equation in one spatial variable, $\phi(x,t)$

$$\frac{\partial \phi}{\partial t} = F(\phi) \frac{\partial}{\partial x} G(\phi) \quad (D-3)$$

The procedure is based on an expansion of nonlinear implicit terms about the known time level, t^n , and leads to a one-step, two-level scheme which, being linear in unknown (implicit) quantities, can be solved efficiently without iteration. The technique is easily extended to treat coupled systems of equations and second-order spatial derivatives. The difference approximation is derived from the following backward time-difference replacement of Eq. (D-3)

$$\frac{\phi_i^{n+1} - \phi_i^n}{\Delta t} = \left[F(\phi) \frac{\partial}{\partial x} G(\phi) \right]_i^{n+1} + O(\Delta t) \quad (D-4)$$

where the spatial differencing of the bracketed term is as yet unspecified. Making use of chain-rule differentiation, the bracketed term in Eq. (D-4) is expanded about t^n ; the result is then differenced using forward time differences and centered spatial differences to obtain the following implicit difference scheme:

$$\begin{aligned} \frac{\phi_i^{n+1} - \phi_i^n}{\Delta t} = & F(\phi_i^n) \delta_x G(\phi_i^n) + \left\{ F(\phi_i^n) \delta_x \left[\left(\frac{\partial G}{\partial \phi} \right)_i^n \left(\frac{\phi_i^{n+1} - \phi_i^n}{\Delta t} \right) \right] \right. \\ & \left. + \left(\frac{\partial F}{\partial \phi} \right)_i^n \left(\frac{\phi_i^{n+1} - \phi_i^n}{\Delta t} \right) \delta_x G(\phi_i^n) \right\} \Delta t \end{aligned} \quad (D-5)$$

On examination, it can be seen that Eq. (D-5) is linear in ϕ^{n+1} and that all other quantities are either known or evaluated at the n level. Because of the spatial difference operator, δ_x , Eq. (D-5) contains ϕ_{i-1}^{n+1} , ϕ_i^{n+1} , and ϕ_{i+1}^{n+1} ; consequently, the system of linear equations generated by writing Eq. (D-5) at each of the grid points, x_i , must be solved simultaneously as an implicit system. The implicit system of equations can be written in tridiagonal matrix form, and can therefore be solved easily and efficiently by standard techniques for tridiagonal systems (see, e.g., Ref. 23). The tridiagonal matrix structure emerges from writing Eq. (D-5) in the following form:

$$a_i^n \phi_{i-1}^{n+1} + b_i^n \phi_i^{n+1} + c_i^n \phi_{i+1}^{n+1} = d_i^n \quad (D-6)$$

where the coefficients contain only n -level quantities. When applied at successive grid points, Eq. (D-6) generates a tridiagonal system of equations for ϕ^{n+1} .

APPLICATION OF THE METHOD

The extension of the numerical method to more than one spatial dimension is based upon an alternating direction implicit (ADI) technique. The technique is an application of the general procedure developed by Douglas and Gunn (Ref. 15) in which the linearization technique described previously is applied to the coupled system of governing equations, Eqs. (24) - (26).

These equations are written in backward time difference form, and non-linear implicit terms are linearized by expansion about t_2^n . The viscous force terms in Eq. (25) which contain mixed derivatives (i.e., $\partial^2 / \partial x_i \partial x_j$ for $i \neq j$) are most easily treated explicitly by evaluation at time level n .

Although mixed derivatives can be differenced implicitly within the Douglas-Gunn framework, this would increase the number of intermediate steps and thereby complicate the solution procedure. Previous experience with the method in Refs. 9, 10 and 18 indicates that the explicit treatment of these viscous terms had no observable effect on stability.

The difference equations obtained by the procedure outlined above represent a linearized backward difference scheme. The equations can be arranged according to time and space derivatives, and written in the following matrix operator form (Ref. 9):

$$\bar{A}^n \left(\frac{\bar{\phi}^{n+1} - \bar{\phi}^n}{\Delta t} \right) = \bar{D}_1^n \bar{\phi}^{n+1} + \bar{D}_2^n \bar{\phi}^{n+1} + \bar{D}_3^n \bar{\phi}^{n+1} + \bar{S}^n \quad (D-7)$$

Here \bar{A}^n is a (mxm) matrix containing the time derivative coefficients, where m is the number of equations being solved; $\bar{\phi}$ is the column vector of the dependent variables; \bar{D}_1^n , \bar{D}_2^n , and \bar{D}_3^n are (mxm) matrices containing three-point difference operators associated with the coordinate directions x_1 , x_2 , and x_3 , respectively; and \bar{S}^n is a column vector containing only n -level terms. Since the multidimensional implicit system with coefficients generated by Eq. (D-7) is difficult to solve, the Douglas-Gunn (Ref. 15) technique is applied to Eq. (D-7) to generate an ADI scheme. With the observation that the Douglas-Gunn procedure is being applied to a coupled system of equations, the following three-step scheme is obtained. (For two spatial dimensions the technique collapses into a two-step scheme.)

$$\bar{A}^n \left(\frac{\bar{\phi}^* - \bar{\phi}^n}{\Delta t} \right) = \bar{D}_1^n \bar{\phi}^* + \bar{D}_2^n \bar{\phi}^n + \bar{D}_3^n \bar{\phi}^n + \bar{S}^n \quad (D-8)$$

$$\bar{A}^n \left(\frac{\bar{\phi}^{**} - \bar{\phi}^n}{\Delta t} \right) = \bar{D}_1^n \bar{\phi}^* + \bar{D}_2^n \bar{\phi}^{**} + \bar{D}_3^n \bar{\phi}^n + \bar{S}^n \quad (D-9)$$

$$\bar{A}^n \left(\frac{\bar{\phi}^{***} - \bar{\phi}^n}{\Delta t} \right) = \bar{D}_1^n \bar{\phi}^* + \bar{D}_2^n \bar{\phi}^{**} + \bar{D}_3^n \bar{\phi}^{***} + \bar{S}^n \quad (D-10)$$

where $\bar{\phi}^*$, $\bar{\phi}^{**}$, and $\bar{\phi}^{***}$ are the intermediate solutions. Note that at each step of the scheme, one more coordinate direction is treated implicitly, and that the most recent approximation to $\bar{\phi}$ is not always used, as this would adversely affect the stability.

The effort involved in the actual programming and solution of Eqs. (D-8) - (D-10) is greatly reduced, and the computer storage requirements are halved by subtracting Eq. (D-8) from Eq. (D-9) and Eq. (D-9) from Eq. (D-10), so that Eqs. (D-9) and (D-10) have the following simplified form:

$$\bar{A}^n \left(\frac{\bar{\phi}^{**} - \bar{\phi}^*}{\Delta t} \right) = \bar{D}_2^n (\bar{\phi}^{**} - \bar{\phi}^n) \quad (D-11)$$

$$\bar{A}^n \left(\frac{\bar{\phi}^{***} - \bar{\phi}^{**}}{\Delta t} \right) = \bar{D}_3^n (\bar{\phi}^{***} - \bar{\phi}^n) \quad (D-12)$$

For three spatial dimensions $\bar{\phi}^{***}$ represents the solution at time $(n+1)$, $\bar{\phi}^{n+1}$; for two spatial dimensions Eq. (D-12) is eliminated and $\bar{\phi}^{**}$ represents the solution.

On examination, it can be seen that the difference equations (D-8), (D-11), (D-12) are linear in the $*$ -level quantities. At the k^{th} step in the procedure there are m equations at each grid point (x_1, x_2, x_3) ; because of the spatial difference operators (δ_k and δ_k^2) these equations contain the dependent variables at x_k and at each of the two adjacent grid points in the x_k -direction. Consequently, the difference equations must be solved as an implicit system. It should be recognized that upon application at a successive number of grid points, x_k , each equation generates a block-tridiagonal system of algebraic equations for $\bar{\phi}^{(k)}$ (i.e., $\bar{\phi}^*$, $\bar{\phi}^{**}$, or $\bar{\phi}^{***}$ FOR $K = 1, 2, 3$). After appropriate treatment of boundary conditions, each system can be solved efficiently using a standard block elimination method such as the matrix factorization method. The method used in the present study is closely related to the matrix factorization method and simply consists of Gaussian elimination for a tridiagonal matrix, but where the elements of the tridiagonal matrix are $(m \times m)$ submatrices rather than scalars, where m is the number of governing equations.

The solution procedure for a single time step is as follows:

- (1) During the first step of the ADI procedure, Eq. (D-8) is applied at successive x_1 -direction rows of grid points to provide one-dimensional implicit systems of equations. These systems are generated by the operator $(\bar{A}^n/\Delta t - \bar{D}_1^n)$. The implicit systems can be arranged in block-tridiagonal form and solved as indicated previously. Since there are m governing equations, the block-tridiagonal systems have (mxm) square matrices as the block elements.

Although this discussion has assumed the grids to be uniform, extension to nonuniform grids is straightforward. When a Roberts transformation is used (see Eqs. (41) - (43)), the first and second derivatives for unequally spaced grid points still lead to three point difference operators. Thus the resulting form of the matrices is unchanged and the solution procedure is identical to that used for the equally spaced case.

SECTION IV
REFERENCES

1. Allen, J. S. and Cheng, S. I., "Numerical Solutions of the Compressible Navier-Stokes Equations for the Laminar Near Wake." Physics of Fluids, Vol. 13, No. 1, January 1970.
2. Baldwin, B. S. and MacCormack, R. W., "Numerical Solution of the Interaction of a Strong Shock Wave with a Hypersonic Turbulent Boundary Layer," AIAA Paper 74-558, AIAA 7th Fluid and Plasma Dynamics Conference, Palo Alto, Calif., June 17-19, 1974.
3. Batham, J. P., "An Experimental Study of Turbulent Separating and Reattaching Flows at High Mach Number," J. Fluid Mech. (1972) Vol. 52, Part 3.
4. Beam, R. M. and Warming, R. F., "An Implicit Finite Difference Algorithm for Hyperbolic Systems in Conservation-Law Form." Paper to be published in Journal of Computational Physics.
5. Bertke, S. D., Werle, M. J. and Polak, A., Finite Difference Solutions to the Interacting Supersonic Turbulent Boundary Layer Equations Including Separation Effects, Dept. of Aerospace Engineering, University of Cincinnati, Ohio, April 1974.
6. Bird, R. B., Stewart, W. E. and Lightfoot, E. N., Transport Phenomena, Wiley, New York, 1960.
7. Bradshaw, P., "The Turbulence Structure of Equilibrium Boundary Layers," Journal of Fluid Mechanics, Vol. 29, 1967.
8. Bradshaw, P. and Ferris, D. H., "Calculation of Boundary Layer Development Using the Turbulent Kinetic Energy Equation: Compressible Flow on Adiabatic Walls." Journal of Fluid Mechanics, Vol. 46, 1971.
9. Briley, W. R. and McDonald, H., "An Implicit Numerical Method for the Multidimensional Navier-Stokes Equations." United Aircraft Research Laboratories Report M911363-6, November 1973.
10. Briley, W. R., McDonald, H. and Gibeling, H. J., "Solution of the Multidimensional Compressible Navier-Stokes Equations by a Generalized Implicit Method," United Technologies Research Center Report R75-911363-15, January 1976.

REFERENCES (Cont'd)

11. Chapman, D. R., Kuehn, D. M. and Larson, H. K., "Investigation of Separated Flows in Supersonic and Subsonic Streams with Emphasis on the Effect of Transition." NACA 1356, January 1949.
12. Coles, D. E., "The Turbulent Boundary Layer in a Compressible Fluid." Rand Report R403 PR, September 1962.
13. Crocco, L. and Lees, L., "A Mixing Theory for the Interaction Between Dissipative Flows and Nearly Isentropic Streams." Journal of the Aeronautical Sciences, Vol. 19, No. 10, October 1952.
14. Curle, N., "The Effects of Heat Transfer on Laminar Boundary Layer Separation in Supersonic Flow." Aero Quarterly, Vol XII, November 1961.
15. Douglas, J. and Gunn, J. E., "A General Formulation of Alternating Direction Methods." Numerische Math., Vol. 6, 1964.
16. Erdos, J. and Pallone, A., "Shock Boundary Layer Interaction and Flow Separation." R.A.E. - TR 61-23, AVCO Corporation, August 1961.
17. Favre, A. J., "The Equations of Compressible Turbulent Gases." Annual Summary Report No. 1, Institute de Mechanique Statistique de la Turbulence, January 1965.
18. Gibeling, H. J., McDonald, H. and Briley, W. R., "Development of a Three-Dimensional Combustor Flow Analysis, Volume I: Theoretical Studies." Air Force Aero-Propulsion Laboratory Report AFAPL-TR-75-59, July 1975.
19. Hafez, M. M. and Cheng, C. K., "Convergence Acceleration and Shock Fitting for Transonic Aerodynamic Computations." University of Southern California Report, USCAE 132, April 1975.
20. Hankey, W. L., Dwyer, D. L. and Werle, M. J., "Branching Solutions for Supersonic Interacting Boundary Layers." AIAA Journal, Vol. 11., No. 9, September 1973.
21. Hankey, W. L. Jr., and Holden, M. S., Two-Dimensional Shock Wave-Boundary Layer Interactions in High Speed Flows. AGARD No. 203, June 1975.
22. Holden, M. S., "Theoretical and Experimental Studies of the Shock Wave-Boundary Layer Interaction on Curved Compression Surfaces." Proceedings of the Symposium on Viscous Interaction Phenomena in Supersonic and Hypersonic Flow. Hypersonic Research Laboratory, Aerospace Research Laboratories, May 1969.

REFERENCES (Cont'd)

23. Isaacson, E. and Keller, H. B., Analysis of Numerical Methods. Wiley, New York, 1961.
24. Klineberg, J. M. and Lees, L., "Theory of Viscous-Inviscid Interactions in Supersonic Flow," AIAA Journal, Vol. 7., No. 12, December 1969.
25. Kreskovsky, J. P., Shamroth, S. J. and McDonald, H., "Application of a General Boundary Layer Analysis to Turbulent Boundary Layers Subjected to Strong Favorable Pressure Gradients," Journal of Fluids Engineering, June 1975.
26. Law, C. H., "Supersonic Shock Wave-Turbulent Boundary Layer Interactions," AIAA Journal, Vol. 14, No. 6, June 1976.
27. Lees, L. and Reeves, B. L., "Supersonic Separated and Reattaching Laminar Flows: I General Theory and Application of Adiabatic Boundary Layer/Shock Wave Interactions." AIAA Journal, Vol. 2, No. 11, November 1964.
28. Lewis, J. E., Kubota, T and Lees, L., "Experimental Investigation of Supersonic Laminar, Two-Dimensional Boundary-Layer Separation in a Compression Corner With and Without Cooling." AIAA Journal, Vol. 6, No. 1, January 1968.
29. MacCormack, R. W. and B. S. Baldwin, "A Numerical Method for Solving the Navier-Stokes Equations with Application to Shock Wave Boundary Layer Interactions." AIAA Paper 75-1, 1975.
30. MacCormack, R. W., "A Rapid Solver for Hyperbolic Systems of Equations," Fifth International Conference on Numerical Methods in Fluid Dynamics, Enschede, Netherlands, June 28-July 3, 1976.
31. McDonald, H., "Mixing Length and Kinematic Eddy Viscosity in a Low Reynolds Number Boundary Layer," United Aircraft Research Laboratories Report J214453-1, September 1970.
32. McDonald, H. and Camarata, F. J., "An Extended Mixing Length Approach for Computing the Turbulent Boundary Layer Development." Proceedings of the AFOSR-IFP-Stanford Conference on Boundary Layer Prediction (Stanford, California), December 1968.

REFERENCES (Cont'd)

33. McDonald, H. and Fish, R. W., "Practical Calculations of Transitional Boundary Layers." International Journal of Heat and Mass Transfer, Vol. 16, No. 9, 1973.
34. McDonald, H. and Kreskovsky, J. P., "Effect of Free-Stream Turbulence on the Turbulent Boundary Layer." International Journal of Heat and Mass Transfer, Vol. 17, No. 7, 1974.
35. Meier, H. V. and Rotta, J. C., "Experimental and Theoretical Investigations of Temperature Distribution in Supersonic Boundary Layers." Preprint No. 70-744, AIAA, 1970.
36. Mikulla, V. and Horstman, C. C., "Turbulence Measurements in Hypersonic Shock-Wave Boundary-Layer Interaction Flows." AIAA Paper 76-162, AIAA 14th Aerospace Science Meeting, Washington, D. C., January 1976.
37. Moretti, G., "Thoughts and After Thoughts About Shock Computations," PIBL Report No. 72-37, Polytechnic Institute of Brooklyn, December 1972.
38. Murman, E. M. and Cole, J. D., "Calculation of Plane Steady Transonic Flow." AIAA Journal, Vol. 9, No. 1, January 1971.
39. Murman, E. M., "Analysis of Embedded Shock Waves Calculated by Relaxation Methods." AIAA Journal, Vol. 12, No. 5, May 1974.
40. Owen, F. K., "Laser Velocimeter Measurements in Free and Confined Coaxial Jets with Recirculation." AIAA Paper 75-120, AIAA 13th Aerospace Sciences Meeting, Pasadena, California, January 20-22, 1975.
41. Reyhner, T. A. and Flugge-Lotz, I., "Interaction of a Shock Wave With a Laminar Boundary Layer." International Journal of Non-Linear Mechanics, Vol. 3, 1968.
42. Roberts, G. O., "Computational Methods for Boundary Layer Problems." Proceedings of the Second International Conference on Numerical Methods in Fluid Dynamics, Springer-Verlog, New York, 1971.
43. Roache, P. J. and Mueller, T. J., "Numerical Solutions of Laminar Separated Flows." AIAA Journal, Vol. 8, No. 3, March 1970.

REFERENCES (Cont'd)

44. Saffman, P. G., "A Model for Inhomogeneous Turbulent Flow." Proc. Roy. Soc., Vol. A317, 1970.
45. Schubauer, C. G. and Tchen, C. M., Turbulent Flow, Princeton University Press, Princeton, New Jersey, 1961.
46. Shamroth, S. J. and McDonald, H., "Assessment of a Transitional Boundary Layer Theory at Low Hypersonic Mach Numbers." NASA CR-2121, November 1972.
47. Shang, J. S. and Hankey, W. L. Jr., "Numerical Solution of the Navier-Stokes Equations for Supersonic Turbulent Flow Over a Compression Ramp." AIAA Journal, Vol. 13, 1975.
48. Shang, J. S., Hankey, W. L. and Law, C. H., "Numerical Simulation of Shock Wave-Turbulent Boundary Layer Interaction." AIAA Paper 76-95, AIAA 14th Aerospace Sciences Meeting, Washington, D. C., January 1976.
49. Sirieix, M., "Decollement Turbulent en Ecoulement Bidimensional." AGARD Conference Proceedings No. 168 on Flow Separation, Gottingen, Germany, May 1975.
50. Smith, A. M. O. and Clutter, D. W., "Solution of the Incompressible Boundary Layer Equations." AIAA Journal, Vol. 1, 1963.
51. Spaid, F. W. and Frishett, J. C., "Incipient Separation of a Supersonic, Turbulent Boundary Layer, Including Effects of Heat Transfer." AIAA Journal, Vol. 10, No. 7, July 1972.
52. Townsend, A. A., "Equilibrium Layers and Wall Turbulence." Journal of Fluid Mechanics, Vol. 11, 1961.
53. Tyson, T. S., "Laminar Boundary Layers in the Neighborhood of Abrupt Spatial Disturbances," Ph.D. Thesis, California Institute of Technology, 1967.
54. Werle, M. J., Dwyer, D. L. and Hankey, W. L., "Initial Conditions for the Hypersonic-Shock/Boundary-Layer Interaction Problem." AIAA Journal, Vol. 11, No. 4, April 1973.

REFERENCES (Cont'd)

55. Werle, M. J. and Vatsa, V. N., "Numerical Solution of Interacting Supersonic Boundary Layer Flows Including Separation Effects." ARL TR 73-0162, Aerospace Research Laboratories, Wright-Patterson AFB, Ohio, December 1973.
56. Wilcox, D. C., "Numerical Study of Separated Turbulent Flows." AIAA Paper 74-584, AIAA 7th Fluid and Plasma Dynamics Conference, Palo Alto, California, June 17-19, 1974.